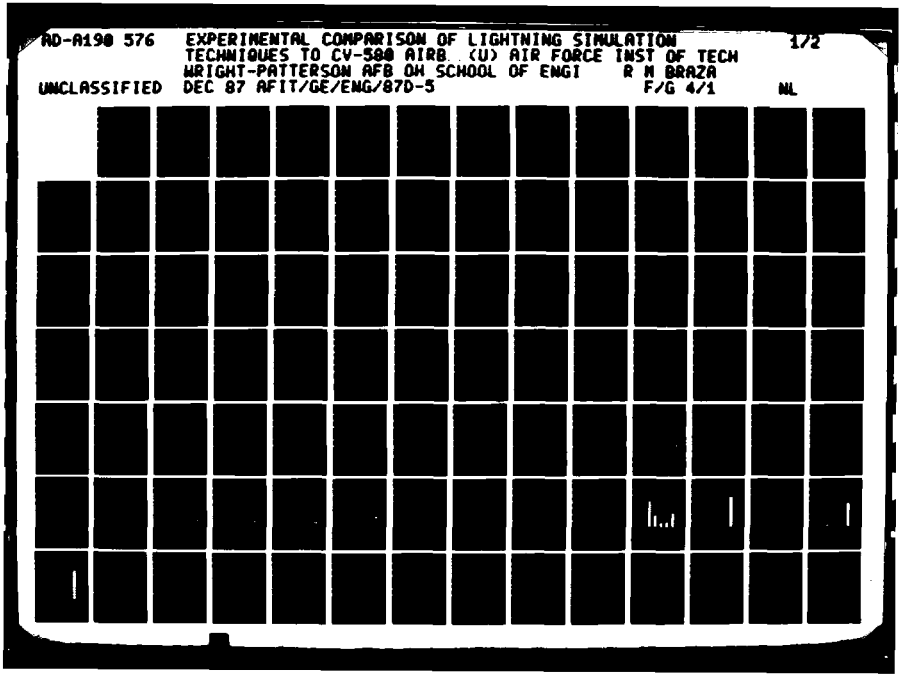
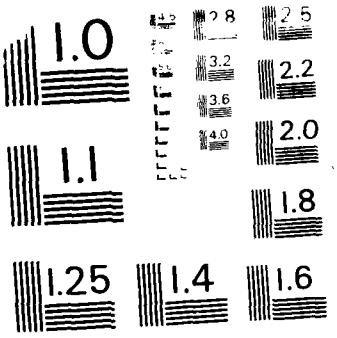
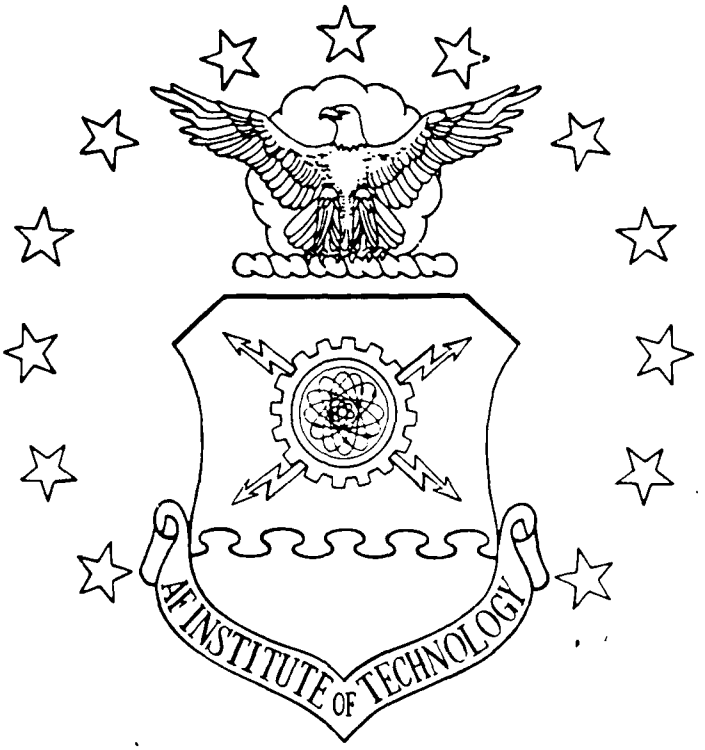

AD-A190 576
EXPERIMENTAL COMPARISON OF LIGHTNING SIMULATION TECHNIQUES TO CV-580 AIRB (U) AIR FORCE INST OF TECH WRIGHT-PATTERSON AFB OH SCHOOL OF ENGI
R M BRAZA
1/2
UNCLASSIFIED
DEC 87 AFIT/GE/ENG/87D-5
F/G 4/1
NL



MICROCOPY RESOLUTION TEST CHART
NATIONAL BUREAU OF STANDARDS-1963-A

DTIC FILE COPY

AD-A190 576



DTIC
ELECTE
APR 01 1988
S D
E

DEPARTMENT OF THE AIR FORCE

AIR UNIVERSITY

AIR FORCE INSTITUTE OF TECHNOLOGY

Wright-Patterson Air Force Base, Ohio

This document has been approved for public release and sale; its distribution is unlimited.

88 3 30 062

AFIT/GE/ENG/87D-5

EXPERIMENTAL COMPARISON OF LIGHTNING SIMULATION TECHNIQUES TO CV-580 AIRBORNE LIGHTNING STRIKE MEASUREMENTS

THESIS

Rudy M. Braza
Second Lieutenant, USAF

AFIT/GE/ENG/87D-5

Approved for public release; distribution unlimited

AFIT/GE/ENG/87D-5

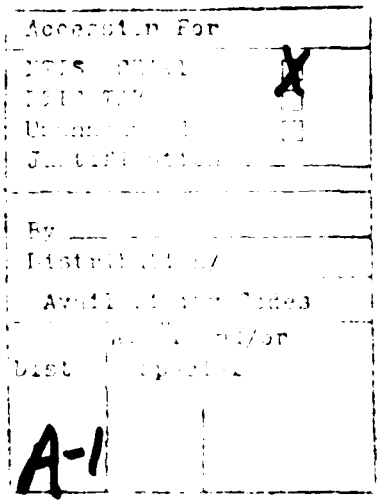
EXPERIMENTAL COMPARISON OF LIGHTNING SIMULATION TECHNIQUES TO CV-580 AIRBORNE LIGHTNING STRIKE MEASUREMENTS

THESIS

Presented to the Faculty of the School of Engineering
of the Air Force Institute of Technology
Air University
In Partial Fulfillment of the
Requirements for the Degree of
Master of Science in Electrical Engineering

Rudy M. Braza
Second Lieutenant, USAF

December 1987



Approved for public release; distribution unlimited

Acknowledgements

In the course of completing my thesis, I have relied upon the assistance of several dedicated people. Foremost, I would like the thank CPT James Hebert, who sponsored my thesis and whose expert advice I found invaluable. I would like to also thank the people at AFWAL/FIESL. I am indebted to their technical expertise in the field of lightning simulation and their patience in assisting my research. Of course, I thank my thesis advisor, CPT Randy Jost, for his guidance and support throughout my research effort. Finally, I thank my family, whose support and encouragement has always been there for me.

Rudy M. Braza

Table of Contents

	Page
Acknowledgments	ii
List of Figures	v
List of Tables	vii
Abstract	viii
1. Introduction	1
Background	2
Lightning	3
Lightning and Aircraft	3
Lightning and Simulation	6
Problem	8
Scope	9
Assumptions	10
Approach	10
Sequence of Presentation	11
2. Theory	13
Overview	13
Lightning Interaction with Aircraft	13
Lightning Simulation and Testing	15
Current Pulse Technique	17
Shock-Excitation Technique	23
Frequency Domain Analysis	28
3. Simulation Measurements	32
Lightning Test Cylinder	32
Return Path	33
Sensors and Data Acquisition	35
Swept Frequency Continuous Wave Test	37
Current Pulse Measurements	40
Shock-Excitation Measurements	47
4. Data Analysis and Comparison	51
Swept Frequency Continuous Wave Data	51
Current Pulse Data	52
Analysis of Shock-Excitation Data	54
Field Responses for Current Pulse	62
Field Responses for Shock-Excitation	65
Comparison of Transfer Functions	66
Full Threat-Level Field Responses	79
Comparison to Airborne Data	89

5. Conclusions and Recommendations 93

Appendix A: Airborne Lightning Measurements 99

Aircraft Instrumentation 99
Ground Station 100

Appendix B: Sensor Specifications 102

Appendix C: Data Acquisition Computer Program 108

Bibliography 116

VITA 119

List of Figures

Figure		Page
1.	Lightning/Aircraft Interaction Process	14
2.	Current Pulse Test Configuration	18
3.	Current Pulse Equivalent Circuit	18
4.	Unipolar Test Waveform	20
5.	Shock-Excitation Test Configuration	25
6.	Tranmission Line Model	25
7.	Lightning Test Cylinder	34
8.	Block Diagram of Data Acquisition System	38
9.	SFCW Test Setup	39
10.	Sensor Locations for SFCW Test	41
11.	Current Pulse Test Setup	42
12.	Unipolar 20 kA Current Pulse	43
13.	Oscillatory Current Waveforms	45
14.	Sensor Locations for Current Pulse Test	46
15.	Shock-Excitation Test Setup	48
16.	Sensor Locations for Shock-Excitation Test	50
17.	P3 SFCW Data	53
18.	P3 20 kA Unipolar Current Pulse Data (H-Field) ..	55
19.	P3 20 kA Unipolar Current Pulse Data (E-Field) ..	56
20.	Typical Shock-Excitation Responses	57
21.	External B-Dot Sensor Response for SE	59
22.	Resulting H-Field Calculation	59
23.	Magnetic Field Lines on Test Cylinder	61
24.	External E-Field Responses for Current Pulse	63

25. External H-Field Responses for Current Pulse 64
26. External E-Field Response for SE 66
27. External H-Field Response for SE 67
28. External H-Field Transfer Function for SFCW 68
29. External H-Field Transfer Function for C20u 69
30. External H-Field Transfer Function for C20o 70
31. External H-Field Transfer Function for C100o 71
32. External H-Field Transfer Function for SE 73
33. External E-Field Transfer Function for C20u 75
34. External E-Field Transfer Function for C20o 76
35. External E-Field Transfer Function for C100o 77
36. External E-Field Transfer Function for SE 78
37. Full Threat-Level Current Waveform Component A .. 80
38. Peak External H-Field Threat-Level Responses 83
39. Peak External E-Field Threat-Level Responses 84
40. Peak Internal H-Field Threat-Level Responses 86
41. Peak Internal E-Field Threat-Level Responses 87
42. Transfer Function for H-Field Airborne Case 92
43. Typical E-Field Waveform for Airborne Strike 97
44. Sensor Locations on CV-580 Aircraft 101

List of Tables

Table		Page
1.	Responses to Threat-Level Current Waveform	82
2.	Measured Peak Field Responses	88
3.	Measured Peak Time Rate-of-Change Responses	90

Abstract

Various lightning simulation test techniques were conducted on the Lightning Test Cylinder developed by the Air Force Wright Aeronautical Laboratories/Atmospheric Electricity Hazards Group (AFWAL/FIESL) and the Air Force Institute of Technology (AFIT/ENG). The experimental tests on the cylinder, which further investigated the assessment of lightning simulation techniques conducted by Butters *et al.*, included swept frequency continuous wave (SFCW), current pulse, and shock-excitation. Designed to model the fuselage of an aircraft, the aluminum test cylinder is over ten meters long with a one meter diameter. To test the effects of various aircraft construction materials, the cylinder was constructed with an aperture where various composite and metal panels can be mounted. The research involved determination of the electric field and magnetic field response transfer functions for each simulation test technique. With these transfer functions, analysis and comparison of the external and internal field responses between the SFCW, current pulse, and shock-excitation tests were made. A major portion of the research was to examine the validity of the linear model for the current pulse simulation technique. In this investigation, transfer functions were derived for various current pulse waveforms. The current waveforms injected into the test cylinder included a 20 kA unipolar, double-exponential pulse and two

oscillatory waveforms with peak amplitudes of 20 kA and 100 kA. The research effort also involved investigation of the induced E-dot (dE/dt) and V-dot (dV/dt) transients of the shock-excitation simulation test for various composite structures. The results of this experimental effort on the Lightning Test Cylinder were then correlated to CV-580 airborne lightning measurements. Differences and similarities between the measured results are presented.

EXPERIMENTAL COMPARISON OF LIGHTNING SIMULATION TECHNIQUES TO CV-580 AIRBORNE LIGHTNING STRIKE MEASURMENTS

1. Introduction

This thesis compares the Current Pulse method with the Shock-Excitation method for the simulation of the airborne aircraft/lightning interaction event. It also provides a comparison of these two test techniques with Swept Frequency Continuous Wave results and CV-580 aircraft in-flight measured lightning strike data. The major tasks accomplished during this thesis effort include:

a. Conducting current pulse simulation tests on the Lightning Test Cylinder using unipolar and oscillatory current waveforms.

b. Conducting shock-excitation tests on the Lightning Test Cylinder.

c. Developing transfer functions of magnetic and electric field responses on the Lightning Test Cylinder for the current pulse, shock-excitation, and swept frequency continuous wave (SFCW) simulation test results.

d. Comparing the temporal and spectral results of the current pulse and shock-excitation simulation tests to CV-580 aircraft lightning strike data.

e. Computing the threat level responses by folding the threat current waveform into the transfer functions that were derived from the lightning simulation tests.

Background

The interest in the electromagnetic interaction of lightning with aircraft is growing due to the increasing use of composite materials, sensitive semiconductor systems, and fly-by-wire technology, particularly in military aircraft. These new aspects in aircraft design raise concern in the susceptibility and vulnerability of aircraft to lightning strikes. Lightning can pose a serious hazard to the safety and operation of aircraft with unprotected avionic, electronic, and fuel systems. Therefore, aircraft design requirements must include the characterization and validation testing of aircraft protection from the lightning threat. The test methods employed to validate lightning protection must reproduce those significant electrical parameters required to simulate lightning effects on aircraft. Two common test methods have been developed to produce these effects: the current pulse (direct injection) method and the shock-excitation method. The current pulse method is most often used by the Air Force and the aerospace industry for lightning protection qualification testing. Some believe that this method does not produce the fast changing electric field changes required to fully simulate

the aircraft/lightning interaction event. Although the differences in these two test methods have been investigated, they have never been specifically evaluated in terms of actual in-flight measured lightning strike data.

Lightning

Uman and Krider describe lightning as a transient, high-current, atmospheric electrical discharge (19:79). Lightning, with its flash of light and associated clap of thunder, occurs when a particular region of the atmosphere attains an electrical charge sufficiently large that the associated electric fields cause an electrical breakdown of the air (19:79). The resulting electric discharge may occur within a cloud (intracloud), cloud-to-cloud (intercloud), or cloud-to-ground (19:79).

Lightning and Aircraft

Aircraft in the vicinity of these highly charged regions are susceptible to being struck by lightning and becoming part of the high current channel. An article by Rustan reports that during 1984 and 1985, the Air Force Wright Aeronautical Laboratory, in conjunction with the FAA, U.S. Navy, NASA, and Office National d'Etudes et de Recherches Aerospatiales (ONERA), obtained direct strike data on an instrumented CV-580 aircraft in order to quantify the lightning threat to aircraft at low altitudes (17:2). A brief discussion of the lightning characterization program

is presented in Appendix A. The maximum levels of the measured parameters were (17:2):

1) peak current: 12 kA
2) rate-of-rise of current: 3.8×10^{10} A/s
3) magnetic flux density derivative: 3950 Wb/m^2s
4) electric flux density derivative: 33 $Coul/m^2s$
5) charge transfer: 103 coulombs
6) pulse repetition rate: 10 kHz

During these two years, the CV-580 was only involved in two confirmed cloud-to-ground lightning strikes. Cloud-to-ground strikes are believed to produce more severe lightning effects than intracloud and intercloud lightning strikes. Tower measurements have shown cloud-to-ground lightning parameters to be more severe than those measured during the in-flight strikes to the CV-580 aircraft (11). Hebert reviewed the results of three in-flight lightning characterization programs and found that the rate at which aircraft are struck by lightning decreases at lower altitudes, but the intensity of the above parameters increases. As altitude increases, the rate of intracloud and intercloud strikes increases while the intensity of the strikes decreases (8). This means that in flying in or near an active thunderstorm, an aircraft is more likely to be struck at higher altitudes, but the intensity of such a strike is likely to be less than at lower altitudes. The

lightning current parameters above, which are present during a lightning strike, result in both direct and indirect effects to the flying aircraft.

The direct effects are primarily produced by the charge and energy transfer during the lightning strike, thereby, causing external physical damage to the aircraft (17:4). The electrical sparkings that can be produced during a lightning attachment, particularly inside the fuel tank of an aircraft, are also considered direct effects (17:4). An article by Plumer and Robb reports that typical direct effects on metallic structures include melting and burnthrough, pitting at structural interfaces, resistive heating, magnetic-force effects, shock wave and overpressure damage, and arcing across bonds, hinges, and joints (14:159-163). On nonmetallic structures, the direct effects of lightning strikes include puncturing of fiberglass or Kevlar reinforced plastics and the delamination and strength degradation of graphite composite structures (14:163-167).

The indirect effects of lightning on aircraft are the induced electromagnetic interactions with aircraft wiring and avionics systems (14:158). This can include inductive and capacitive coupling mechanisms. The indirect effects are determined from the relationship between the surface currents and charge densities throughout the aircraft surface and the induced transients on the wiring and avionics systems (17:4).

Perala and DuBro point out that aircraft/lightning interaction events are the result of the high voltage phase and high current phase of the lightning strike (12:3). The high voltage phase occurs when the lightning channel initially attaches to the aircraft (12:3). During this phase, there is a rapid rise and time rate-of-change in the electric fields and a relatively small current induced on the aircraft surface (12:3). This is followed by the high current phase, which occurs when the return stroke propagates through the lightning channel (12:3).

Lightning and Simulation

Because of the complexity of the aircraft/lightning interaction process, it is necessary to use ground lightning simulation and testing to assess the effects of lightning on aircraft. Laboratory lightning simulation does not attempt to actually reproduce the entire natural lightning event, since natural lightning is a highly varying, discontinuous, and complex phenomenon. Rather, the purpose of lightning simulation is to generate those electrical parameters which reproduce the direct and indirect effects of lightning on aircraft. A report by Butters *et al.* (2) describes two major lightning simulation techniques which have been developed to produce lightning's most significant electrical parameters: current pulse and shock-excitation.

The current pulse technique is performed by injecting a low-level (or high-level) current pulse waveform through the

test aircraft (2:1). In the low-level case, the resulting induced transients are measured and then linearly scaled to the required threat levels (2:1). When moderate threat waveforms (30,000 Amperes) are injected, only minor scaling is required. When full threat pulses (200,000 Amperes) are injected, no scaling is required. It should be noted that there are only two lightning simulators in the United States capable of injecting the full threat pulse into a fighter sized aircraft or larger: one at Sandia National Laboratories and one developed by the Air Force in its Atmospheric Electricity Hazards Protection Advanced Development Program (7). The majority of current pulse lightning simulation tests are performed at reduced current levels and the resulting transients are linearly scaled to the full threat level. With this technique, a current impulse generator and a waveforming network are attached to the aircraft test body (2:3). The current return path is then wired from the aircraft back to the generator (2:3).

The shock-excitation technique is a recent development in lightning simulation technology. This technique uses spark gaps to isolate the aircraft test body from the generator and ground (2:1). The shock-excitation technique discharges a high voltage generator (a Marx bank) to break down the air between the gaps and to provide both current and voltage excitation (2:1). The result is reported to reproduce the effects of several lightning strike events:

the rapid change of the electric fields, the lightning attachment, and the return stroke (2:1).

In comparing the two lightning simulation techniques, Butters points out that the current pulse technique assumes dominant inductive coupling mechanisms and the absence of nonlinear lightning effects (2:1). However, higher current levels result in nonlinear effects and deviate from the linear scaling analysis (2:3). But, it is argued that these deviations will result in a more conservative linear analysis of the lightning effects on the aircraft (2:3). Perala and DuBro state that the current pulse technique simulates only the high current phase of the lightning strike; whereas, the shock-excitation technique simulates both the high current and high voltage phases, and also addresses the analysis of the nonlinear effects (12:3,5).

Problem

The overall goal of this thesis is to assess the capabilities of the current pulse and the shock-excitation simulation methods to produce the significant lightning electrical parameters, which contribute to the airborne aircraft/lightning interaction event. Specifically, the objective is to determine the answers to the following questions:

a. How do the transients for the current pulse and shock-excitation simulation techniques compare to swept

frequency continuous wave measurements when linearly scaled to the full threat level?

b. Is the current pulse method alone sufficient to assess the susceptibility/vulnerability of an aircraft to the lightning threat?

c. Does the current pulse method faithfully reproduce all of the significant effects recorded during the in-flight lightning strikes to the CV-580?

d. What significant effects, if any, are not reproduced by the current pulse method and can only be produced by using the shock-excitation method?

Scope

Although there are several variations associated with lightning simulation techniques, this thesis will only investigate the current pulse simulation technique using unipolar and oscillatory waveforms, the shock-excitation simulation technique, and the SFCW technique. The simulation tests are conducted on the Lightning Test Cylinder. Also, there have been several in-flight lightning characterization programs prior to the CV-580 program during 1984 and 1985. The current pulse and shock-excitation simulation techniques will only be compared with the data measured and recorded by the CV-580 lightning characterization program. The parameters that will be used for comparison in this thesis are limited to the maximum measured and computed levels of the E-field, H-field, time

rate-of-change of the E-field (dE/dt), time rate-of-change of the H-field (dH/dt), and current. Frequency domain comparisons will only be directed to spectral distributions of the transfer functions for the airborne measurements and each of the simulation techniques.

Assumptions

One key assumption necessary for this thesis is that the induced transients of the aircraft/lightning interaction event can be linearly extrapolated to the full threat level. Therefore, the interaction event can be modeled as a linear, time invariant system with the use of transfer functions. Another required assumption is that a digital sample rate of 5 nanoseconds for a 10 microsecond window is sufficient for the data acquisition equipment to record the significant interaction effects during the in-flight tests and the lightning simulation tests. Also, an assumption is made that the CV-580 data is representative of a lightning interaction event with an airborne aircraft.

Approach

The approch of this thesis is to experimentally and analytically determine which test method most faithfully reproduces lightning interaction's most significant effects by making both time domain and frequency domain comparisons of the current pulse and shock-excitation tests to the CV-580 airborne measurements. The first part of the thesis

involves conducting experimental tests on the Lightning Test Cylinder developed by the Air Force Wright Aeronautical Laboratories -- Atmospheric Electricity Hazards Group (AFWAL/FIESL) and the Air Force Institute of Technology (AFIT). The experimental tests on the test cylinder include current pulse and shock-excitation lightning simulations and swept frequency continuous wave measurements. From these experimental measurements, the response transfer functions of the test cylinder from each test are then developed. With the transfer functions, analysis and comparisons of the responses beween the SFCW, current pulse, and shock-excitation tests to the threat level lightning waveform can be made.

The second part of this thesis is comparison to the CV-580 airborne lightning strike data. The transfer function of the aircraft's response to an actual lightning strike is compared to those of the current pulse and shock-excitation lightning simulation methods. Lightning interaction effects are analyzed by comparisons and evaluations of transfer functions between induced transients external and internal to the test cylinder.

Sequence of Presentation

This thesis is developed in several distinct sections. In Chapter 2, the elementary theory necessary to understand the basic interaction process of lightning with aircraft and

the lightning simulation techniques is presented. The experimental procedures and data acquisition of the lightning simulation measurements are discussed in Chapter 3. Chapter 4 presents comparisons and analysis of the experimental results with the airborne lightning strike data. Conclusions and recommendations are discussed in Chapter 5.

2. Theory

Overview

An understanding of the basic interactions of lightning with aircraft and the simulation techniques to reproduce lightning's significant effects is necessary for the development of this thesis. This chapter will present and review the lightning/aircraft electromagnetic interaction process, lightning simulation requirements, the current pulse technique, the shock-excitation technique, and frequency domain analysis methods.

Lightning Interaction with Aircraft

The interest in the electromagnetic interaction of lightning with aircraft is increasing due to the growing use of composite materials, sensitive semiconductor systems, and fly-by-wire technology. This section will review the fundamentals of the interaction process. An extensive review of state of the art lightning interaction modeling has been written by Perala, Rudolph, and Eriksen (13).

The lightning/aircraft electromagnetic interaction process is often considered as three separate processes: external interaction, internal interaction, and internal propagation. Although these three processes are analyzed individually, theoretically they are not separate (13:173). The interaction process can be analyzed separately, however, when there is very little mutual coupling between the

various processes (13:173). Figure 1 illustrates the interaction process with an aircraft attached to a lightning channel.

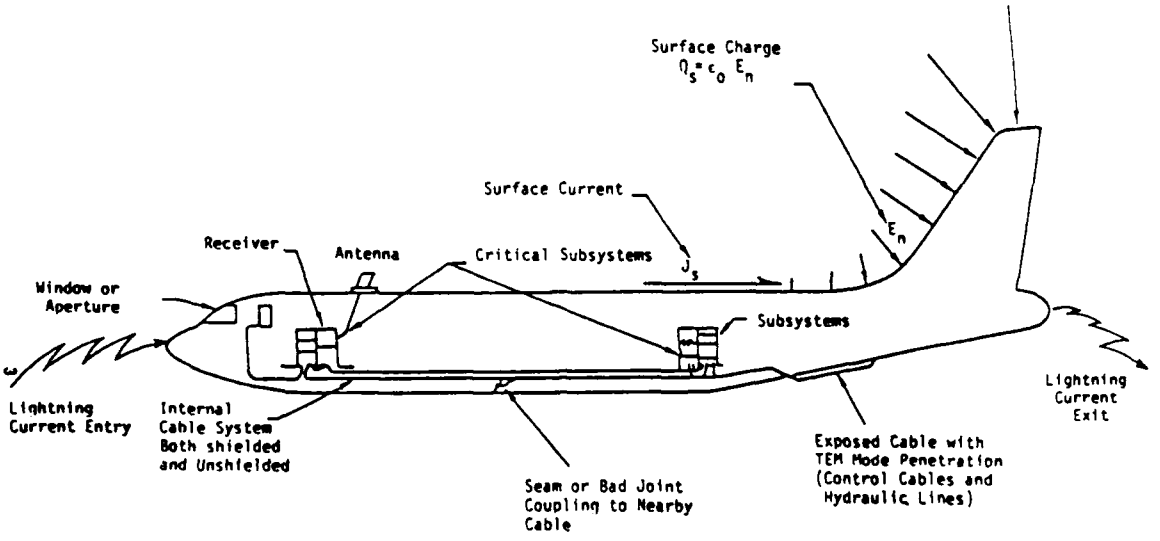


Figure 1. Lightning/Aircraft Interaction Process (13).

The first part of the process, the external interaction, is initiated when the lightning channel induces a surface current density and a charge density which results from the flow of electrical charge on the aircraft surface. The surface current and charge densities respectively correspond to the tangential magnetic fields and normal electric fields on the surface of the aircraft (13:173).

Internal interaction is the second part of the lightning/aircraft interaction process. It is the penetration of lightning energy into the interior of the aircraft due to apertures, antennas, exposed cables and conductors, panel seams and joints, and skin diffusion of the aircraft (13:173).

The final part of the interaction process, internal propagation, follows once the lightning energy penetrates through the shell of the aircraft. In general, the aircraft's internal wiring, metallic fluidlines, and control cables act as transmission lines through which the lightning energy effectively propagates, ultimately to critical electronic systems (13:173).

Lightning Simulation and Testing

Ground lightning simulation and testing are used to assess the effects of lightning on aircraft and to validate lightning protection for aircraft. The goal of lightning simulation is not to reproduce the entire natural lightning event, but to accurately simulate or reproduce the significant direct and indirect effects of lightning on aircraft. The simulation of these direct and indirect effects are often based on the production of four of lightning's electrical parameters (6:2):

1) the current peak amplitude (Imax)

2) the maximum current rate of change (dI/dt)

3) the charge transfer ($\int$ idt)

4) the action integral ($\int i^2 dt$)

The action integral ($\int i^2 dt$) represents the lightning pulse's ability to dissipate or deliver energy to the aircraft or test body (3:209). In general, lightning simulation and testing programs incorporate statistical combinations of the four above parameters in order to characterize the lightning interaction event (6:2).

Criteria for military lightning simulation testing is documented in MIL-STD-1757A, which presents the waveforms to be used in laboratory lightning simulation tests and for lightning protection qualification of military aircraft. MIL-STD-1757A specifies the following test waveforms (3:210):

1) Voltage Waveform A: for punch-through/flashover testing; a 1000-kV/μs ramp until breakdown.

2) Voltage Waveform B: dielectric testing and fuel ignition testing; 1.2 μs time-to-peak and 50 μs time-to-decay to 50 percent.

3) Voltage Waveform C: attach-point testing; 2 μs time-to-peak.

4) Voltage Waveform D: attach-point testing; 50 μs time-to-peak.

5) Current Waveform A: initial stroke component.

6) Current Waveform B: intermediate current component.

7) Current Waveform C: continuing current component.

8) Current Waveform D: restrike component.

9) Current Waveform E: magnetic-coupling testing.

Typically, these waveforms are utilized and applied to test aircraft by appropriately time sequencing the various waveform components (3:210). The test waveforms are not designed to replicate natural lightning itself, but to simulate the direct and indirect effects caused by the lightning event (3:211). Note that while many lightning simulation tests which employ the current pulse (direct injection) method concentrate primarily on the current waveform components presented above, the military standard includes voltage waveforms as well.

Current Pulse Technique

The current pulse technique, also known as the lightning transient analysis (LTA) technique, was originally developed by the General Electric High Voltage Laboratory (15:15). It is performed by injecting a current pulse -- low-level, moderate-level, or full threat-level -- through the structure of the test aircraft (2:1). With this technique, a current impulse generator (a capacitor bank) and a resistive waveshaping network are attached directly to the aircraft test body at an entry point (2:3; 21:450). The current return path for the setup is then hard-wired from the exit point on the aircraft back to the generator (2:3). The test configuration is often modelled as a simple series RLC circuit (21:450). Analytically, the inductance of the configuration is assumed to be determined by a combination

of the current return path and the test aircraft (21:450). The waveshaping network and the current generator determine the resistance and the capacitance of the system respectively (21:450). An example of the current pulse setup -- a test on the F-16 by AFWAL -- and its equivalent circuit are illustrated, respectively, in Figures 2 and 3.

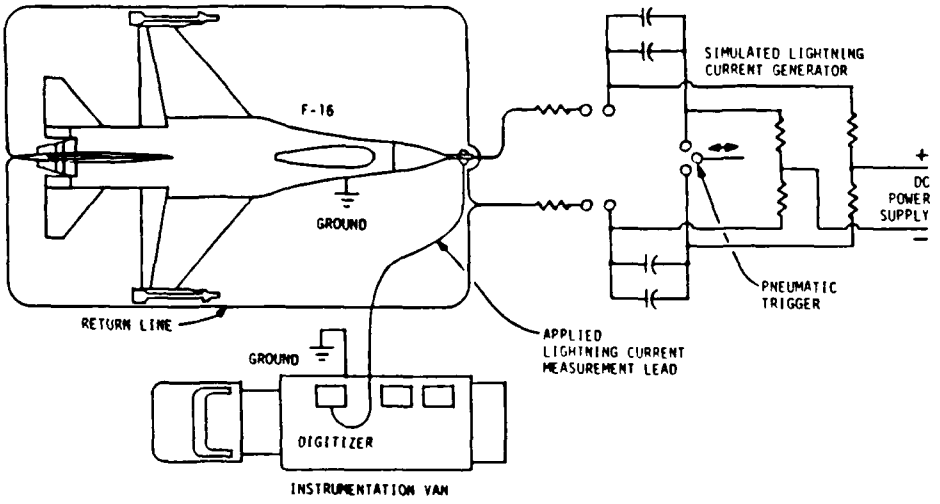


Figure 2. Current Pulse Test Configuration (21:456)

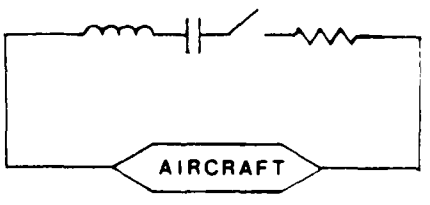


Figure 3. Current Pulse Equivalent Circuit (15:16)

The parameters of the configuration are chosen such that a unipolar, double exponential, impulse current waveform is injected through the aircraft structure (21:450). The equations describing the injected current waveform are given by (21:450)

$$i(t) = \left(\frac{V}{2kL}\right)\left[e^{(k-a)t} - e^{-(k-a)t}\right] \tag{1}$$

$$a = \frac{R}{2L} \tag{2}$$

$$k = \left[a^2 - \frac{1}{LC}\right]^{1/2} \tag{3}$$

where

i(t) = time varying current (amperes)

V = capacitor voltage (volts)

L = circuit impedance (henries)

R = circuit resistance (ohms)

C = circuit capacitance (farads)

The resulting normalized waveform, marked by the rise time (t_r) and decay time (t_t), is illustrated in Figure 4.

Most often the current pulse technique is used to inject a low threat-level or moderate threat-level current waveform from which the resulting induced transients are linearly extrapolated to full threat levels, typically a current peak of 200 kA (21:449). In order to simulate the

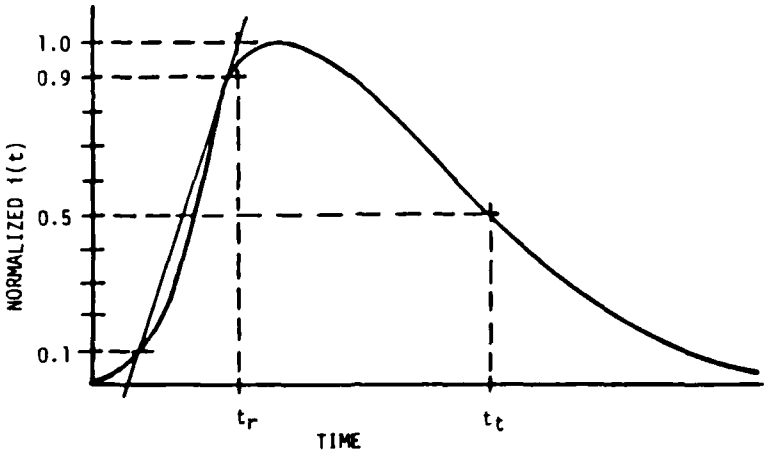


Figure 4. Unipolar Test Waveform (21:456).

lightning/aircraft interaction event, MIL-STD-1757A and data from statistical lightning characterizations require the following criteria for the current pulse waveform (21:451):

I_p = 30 kA (moderate threat-level peak current)

t_r = 2 μs ± 20% (10% to 90% rise time)

t_t = 50 μs ± 20% (50% tail time)

The resistive, capacitive, and inductive components of the test configuration are selected to maintain the peak current I_p while keeping the waveform within the required tolerances (21:452). Computer numerical techniques are used to optimize the test configuration by determining the required

values of the components (21:452). Using the Kirchoff voltage equation, the test configuration equivalent circuit produces the following series RLC equation at time $t = 0^+$ (21:452):

$$V = (1/C)\int i(t)dt + R\left[i(t)\right] + L\left[di(t)/dt\right] \qquad (4)$$

whose time derivative is given as:

$$0 = (1/C)\left[i(t)\right] + R\left[di(t)/dt\right] + L\left[d^2i(t)/dt^2\right] \qquad (5)$$

For full scale lightning tests on the F-16 aircraft, the current pulse test setup at AFWAL's Flight Dynamics Laboratory uses two banks of capacitors with a total capacitance of 8.4 microfarads (21:453). The configuration is improved by utilizing a pneumatic spark gap system that closes until sparkover between the two banks to produce a cleaner current waveform (15:19; 21:454). The current is then damped by a resistive network of 3 ohms at the generator output (21:453). Another improvement of the current pulse technique at the Air Force Flight Dynamics Laboratory is the use of multiple return paths (15:19; 21:450-451). The multiple paths more evenly distribute the field around the test aircraft and reduce the inductance of the system to obtain a higher peak current (21:450-451). By utilizing four aluminum return paths, the overall inductance

of the configuration with the F-16 aircraft is approximately 3.5 microhenries (21:454). In measuring the induced transients from lightning/aircraft coupling, the current pulse simulation setup at the Flight Dynamics Laboratory incorporates a transient digitizer to provide spectral data on the phase and amplitude of the driving current and response (15:19). From this information, the actual transfer function of the test configuration is then determined and appropriately identified in the analysis of the results (15:19).

In the current pulse lightning simulation technique, the resulting measured induced transients from the injected low-level, or moderate-level, current pulse are linearly scaled to full threat levels where resistively-coupled transients are extrapolated from the peak current and inductively-coupled transients are extrapolated from the current time rate-of-change. The current pulse technique assumes that linear extrapolation of the induced transients is valid if the injected current waveform is identically scaled to the full threat lightning waveform (2:1,3).

From analytical and experimental investigations, McCormick, Maxwell, and Finch report on the validity of the current pulse (LTA) technique (10). In the research program sponsored by the Air Force Flight Dynamics Laboratory, lightning simulation test (LST) data is used to derive the transfer function of the test configuration (10). Using the

time and frequency domain inputs derived from the LST data, it was concluded that the LTA technique is a valid method for assessing the susceptibility and vulnerability of aircraft to the effects and hazards of lightning (10:142). The results also determined that the linearity of the current pulse configuration is a valid and justified assumption, and that linear extrapolation to the full threat lightning level is an appropriate analysis (10:134,142).

Shock-Excitation Technique

The shock-excitation technique, developed by the McDonnell Aircraft Company, differs from the current pulse technique by using spark gaps to electrically isolate the aircraft test body from the generator and ground (2:1; 15:23). The shock-excitation setup incorporates these large input and output spark gaps on the test aircraft to produce both charging transients and discharging transients. A high voltage Marx generator is used to break down the air between the spark gaps and to provide both current and voltage excitation to the aircraft (2:1). A Marx bank is a simple pulsed power generator in which N capacitors are charged in parallel to a given voltage, V_o. The capacitor bank is then discharged in series to achieve very high voltages; ideally, $N \times V_o$ volts. The arc breakdown of air occurs at approximately 10 kilovolts per centimeter. Therefore, an airgap of 1 meter requires approximately one million volts to break down.

In the sequence of events during the shock-excitation simulation, the discharging Marx generator produces a rapidly changing E-field between the input electrode and the test body. After a few microseconds, an arc will be established which will produce a rapid charging of the body. A second arc will then be established from the body to ground -- rapidly discharging the vehicle. The two arcs will complete the circuit of the test setup and allow the Marx generator to discharge a high current through the vehicle. Because of the finite amount of time required for the long arcs to be established, various transient mechanisms are simulated. Reportedly, the different mechanisms simulated with the shock-excitation technique are: (1) nearby lightning from the rapidly changing E-field, (2) stepped-leader attachment from the charging of the aircraft, and (3) return stroke from the discharging of the test vehicle (2:1). The McDonnell Aircraft Company shock-excitation test setup is illustrated in Figure 5.

The shock-excitation configuration and the resulting coupling to internal wiring are modeled analytically as two coupled transmission line circuits, as shown in Figure 6, where one circuit represents the aircraft test body and the other represents the internal wiring of the aircraft (2:12-13). The generator and the waveshaping network are modeled as lumped parameters (2:12). A time-varying arc resistance is used to model the spark gaps in the test

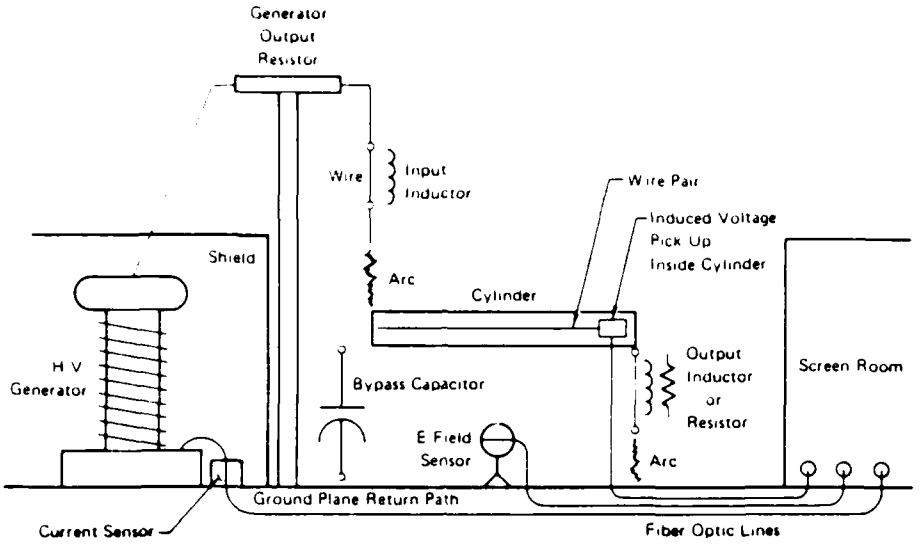


Figure 5. Shock-Excitation Test Configuration (2:5)

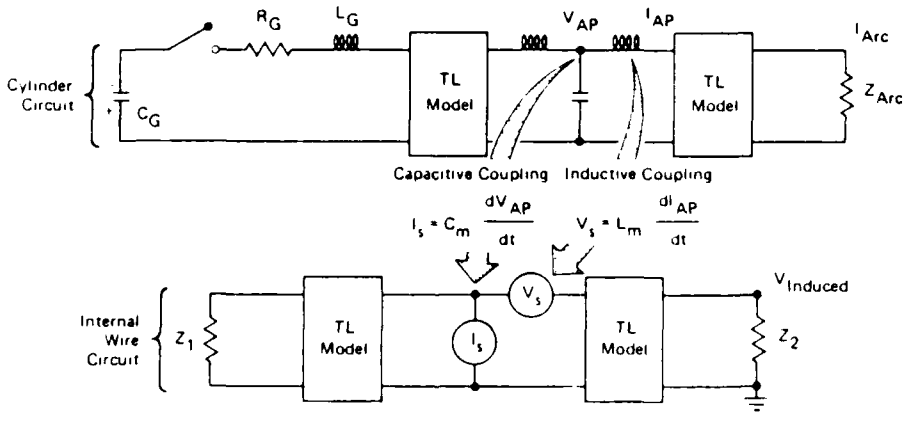


Figure 6. Transmission Line Model (2:13)

configuration (2:12). The capacitive and inductive coupling mechanisms are modeled, respectively, as a parallel current source I_S and a series voltage source V_S in the equivalent circuit of the internal wiring (2:13).

The shock-excitation lightning simulation can be divided into a charging phase and a discharging phase (2). The charging phase in essence simulates the stepped-leader attachment of the lightning strike, and the discharging phase simulates the return stroke (2:37). The charging phase is simulated by isolating the aircraft test body from ground potential and then switching the high-voltage generator output to the test body (2:37). The high voltage potential of the generator induces the flow of displacement currents on the surface of the test body, thus, quickly charging the aircraft structure to a high potential (2:37). The resulting currents and voltages on the test body during the charging phase is modeled from a series RLC circuit (2:15,38). The current and voltage waveforms are given respectively as (2:15,38):

$$i(t) = (V/wL)\, e^{-at} \sin(wt) \tag{6}$$

and

$$V(t) = (1/C_c) \int i(t)dt \tag{7}$$

where

$a = R/2L$

w = frequency (radians/sec)

V = generator voltage (volts)

C_c = test body capacitance (farads)

L = total inductance (henries)

R = series resistance (ohms)

The time derivatives of the current and voltage waveforms are given respectively as (1:38):

$$di(t)/dt = (V/wL)\left[(w)\cos(wt)-(a)\sin(wt)\right]e^{-at} \quad (8)$$

and

$$dV(t)/dt = i(t)/C_c \quad (9)$$

Following the charging phase, the discharging phase of the shock-excitation technique simulates the return stroke of the lightning strike (2:51). During the charging phase, the test body is charged to a high potential due to high electrical fields produced by the Marx generator's output and due to the output spark gap isolating the test body from ground potential (2:51). The discharge phase occurs once the output spark gap breaks down and the test body is then quickly discharged to ground potential (2:51). This rapid

discharge produces very high dE/dt's of approximately 10^{12} V/m/s (2:51).

Frequency Domain Analysis

Frequency domain, as well as time domain, techniques are used in this thesis for the analysis of measurements from the CV-580 airborne lightning program, the current pulse tests, and the shock-excitation tests. In the first part of the analysis, frequency domain techniques are applied to the measured data to determine the actual response of both the airborne and simulated lightning/aircraft interaction events. The measured sensor data not only records the electrical phenomena, but also the particular characteristics of the sensor. A more accurate characterization of the electrical phenomena is provided by isolating and removing the effects of the measurement system from the data (6:5). First, frequency domain transfer functions of each component in the measurement system are determined by a Hewlett-Packard 3577A network analyzer. The components of the measurement system include electric field, magnetic field, and current sensors with fiber optic links. The network analyzer measures the response of each measurement system component to a swept frequency continuous wave (SFCW) signal, from DC to the upper frequency limit associated with the component (6:5). The ratio of the response to the CW signal at discrete frequencies produces

the corresponding frequency domain transfer function of each component in the measurement system (6:5).

The measured time domain transients due to lightning interaction effects are also transformed into the frequency domain by using the Fast Fourier Transform. Dividing out the transfer functions of the measurement system components from these measured transients produces the actual lightning response in the frequency domain. An inverse of this corrected frequency transform results in the actual time domain signal by removing the effects of the measurement system (6:5).

An advantage of this procedure is that the response of a derivative field sensor, electric or magnetic, is integrated in the time domain, as well as removing the effects of the measurement system. In the frequency domain, dividing out the transfer function of the derivative measurement component corresponds to integration in the time domain.

The second part of the frequency domain analysis is to produce the transfer functions of the CV-580 aircraft and the test object at the various sensor locations. The transfer functions that are developed relate the response of the system to airborne or simulated lightning strikes. This is shown in the following relationship (6:5):

$$T(\omega) = R(\omega)/S(\omega) \qquad (10)$$

where

$T(\omega)$ = frequency domain transfer function

$R(\omega)$ = Fourier transform of actual sensor response

$S(\omega)$ = Fourier transform of applied excitation source

The response transfer function $T(\omega)$ contains both amplitude and phase information. They are produced for the SFCW, current pulse, shock-excitation, and airborne cases at each sensor location. The excitation source, as well as the sensor response, may be voltage, current, electric field, or magnetic field.

Once the transfer function is determined it is possible to analytically determine what the transient response at a particular location would be to various threat waveforms. This is shown by the following relationship:

$$R_T(\omega) = I_T(\omega)\ T(\omega) \qquad (11)$$

where

$R_T(\omega)$ = response to threat waveform

$I_T(\omega)$ = threat waveform

$T(\omega)$ = transfer function

By taking the inverse Fourier transform of $R_T(\omega)$, it is possible to obtain the time domain transient response to the threat waveform.

It is important to realize that the frequency domain analysis using the Fourier transform assumes a linear time-invariant system. Therefore, the key assumption in the analysis is that the lightning interaction event is a linear process and neglects nonlinearities such as arcing, corona, streamering, and surface tracking. It is argued, however, that these mechanisms result in losses of electromagnetic energy and that an assumption of linearity will result in a more conservative analysis of the lightning interaction event -- predicting higher values than if the nonlinearities are taken into consideration (2:3). Actual tests at very low level SFCW inputs of about 25 watts, followed by current pulse tests at 20,000 amperes, showed that the extrapolation was conservative in the majority of cases during lightning simulation tests on an F-14 fighter aircraft (5). Because of the exceptions to the case and the importance of validated lightning protection, extreme care must be exercised in applying frequency domain techniques for actual lightning protection qualification testing when low level currents are used. In general, when applied to transient reponses recorded during current pulse tests, the less the extrapolation necessary, the better (5).

3. Lightning Simulation Measurements

This chapter describes the experimental phase of this thesis. It discusses the procedures and equipment of the simulation tests that were conducted on the Lightning Test Cylinder at AFWAL/FIESL. The lightning simulation techniques conducted on the Lightning Test Cylinder were Swept Frequency Continuous Wave, Current Pulse, and Shock-Excitation. The resulting magnetic fields, electric fields, and currents induced on the cylinder are recorded for each test technique.

Lightning Test Cylinder

The Lightning Test Cylinder is the test bed that was used for the lightning simulation experiments performed for this thesis. The cylinder was fabricated by the Air Force Institute of Technology Fabrication Shop out of 0.060 inch thick sheet aluminum using aircraft construction techniques. Designed to model the fuselage of an aircraft, the cylinder is over ten meters in length with a diameter of one meter. In order to determine the shielding effectiveness and the entry of electromagnetic energy through various aircraft construction materials, the cylinder was built with an aperture in the center. The aperture is 1.5 meters long and spans one-third of the circumference of the cylinder. A variety of panels can then be fastened over this aperture. The panels used in this thesis include one solid aluminum

panel, which is identical to the material of the cylinder, and two graphite composite panels. One of the composite panels is composed of nickel-coated carbon fibers and is identified in this thesis as Composite #1. The other composite panel, which is identified as Composite #2, is also composed of nickel-coated carbon fibers and has a copper mesh imbedded in the surface of the panel. The tests were also conducted with an open aperture, using no panel.

Return Path

A coaxial return path was used for the Swept Frequency CW and Current Pulse tests. The coaxial return path provides a uniform electromagnetic field distribution around the cylinder. The coaxial return path is approximately 14 meters long with a diameter of 2.3 meters. The return path over the center part of the cylinder, where the aperture is located, is fabricated out of sheet aluminum, 2.4 meters long. The remainder of the cylindrical section of the return path is constructed out of wire mesh with the wires spaced about 10 cm apart along the axis and about 5 cm apart around the circumference of the cylinder. The wire spacing for the two conical sections of the coaxial return path is about 20 cm along the cylinder axis. Figure 7 illustrates the Lightning Test Cylinder with the coaxial return path. A flat ground plate return path, however, was used for the Shock-Excitation test. The flat ground plate return, rather

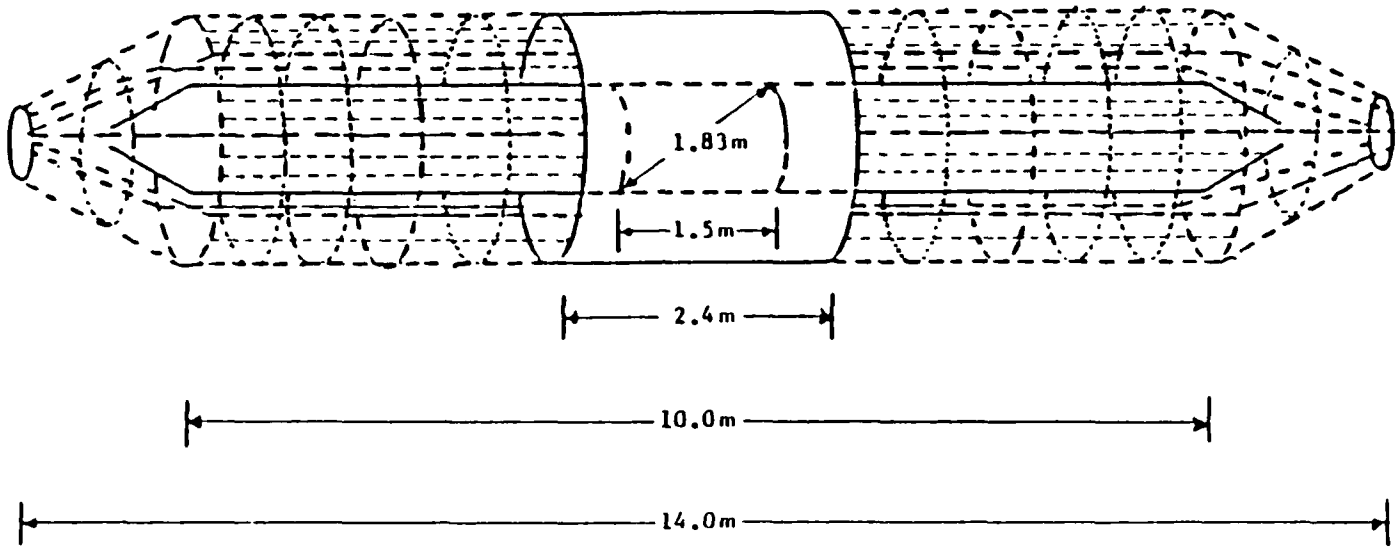


Figure 7. Lightning Test Cylinder with Coaxial Return Path.

than the coaxial return, was used to avoid possible arcing between the cylinder and return path by the high voltage Marx generator during the Shock-Excitation test.

Sensors and Data Acquisition

The electric field (D-dot) and magnetic field (B-dot) sensors used in the lightning simulation tests are derivative sensors, which respond to the time rate-of-change of the corresponding field. The field sensors, manufactured by EG&G, are passive devices, requiring no external power. The pertinent equation characterizing the response of the B-dot sensors is

$$V_O = A_{EQ}(dB/dt) \tag{12}$$

For the D-dot sensor, the response is given as

$$V_O = R\ A_{EQ}(dD/dt) \tag{13}$$

where

V_O = output voltage (volts)

A_{EQ} = sensor equivalent area (m^2)

R = sensor characteristic load impedance (ohms)

B = magnetic flux density (webers/m^2)

D = electric flux density (coulombs/m^2)

In addition to the electric and magnetic field measurements, the current levels on the cylinder are also measured by a current transformer for the Current Pulse test and by a current shunt for the Shock-Excitation test. The specifications for the sensors used in this thesis are provided in Appendix B.

The output response of each sensor is fed into a fiber optic transmitter, which convert the sensor's electrical response to an optical signal. The fiber optic transmitters are battery operated and are activated pneumatically. Because of the severe electromagnetic environment generated during the lightning simulation tests, the fiber optic links were used to eliminate common mode interference and ground loop problems (2:107). A total of four fiber optic links were used. The fiber optic transmitters themselves were shielded to reduce noise pickup. Noise checks were performed for each simulation setup to insure that the transmitters were not affected by any noise, such as electromagnetic interference from surrounding sources.

Fiber optic cables linked the transmitters to fiber optic receivers located in an EM-shielded instrumentation room. The receivers converted the optical signals back to electrical sensor responses. The sensor responses are fed into two 2-channel Tektronix 7612D waveform digitizers. The digitizers, which are triggered by one of the sensors, are set to read the data at 2048 samples with a sampling

interval of 5 nanoseconds. This provides a 10.24 microsecond data window with a frequency response of 100 MHz. The sampling rate is identical to the digital data of the airborne lightning measurement program. The data from the digitizers were then read into a Digital PDP 11/34 computer and recorded on 9-track magnetic tape. The PDP 11/34 computer controls data acquisition and subsequently performs data reduction. A block diagram of the data acquisition system is depicted in Figure 8. A listing of the computer program used for data acquisition is provided in Appendix C.

Swept Frequency Continuous Wave Test

The SFCW test measurements were conducted by Captain Randy J. Jost of AFIT/ENG. Some of the results of his measurements are incorporated into this thesis. The setup of the SFCW test is depicted in Figure 9. With a radius ratio of 2.3, the cylinder and the coaxial return path represent a coaxial transmission line with a characteristic impedance of approximately 50 ohms. A 50 ohm matched load, therefore, is placed between the cylinder and the return path in order to eliminate reflected waves.

A Hewlett-Packard 3577A network analyzer is the heart of the SFCW system. It generates a CW current, swept from DC to 100 MHz, which is amplified and injected through the cylinder. An EG&G CML-7 B-dot sensor is then used to

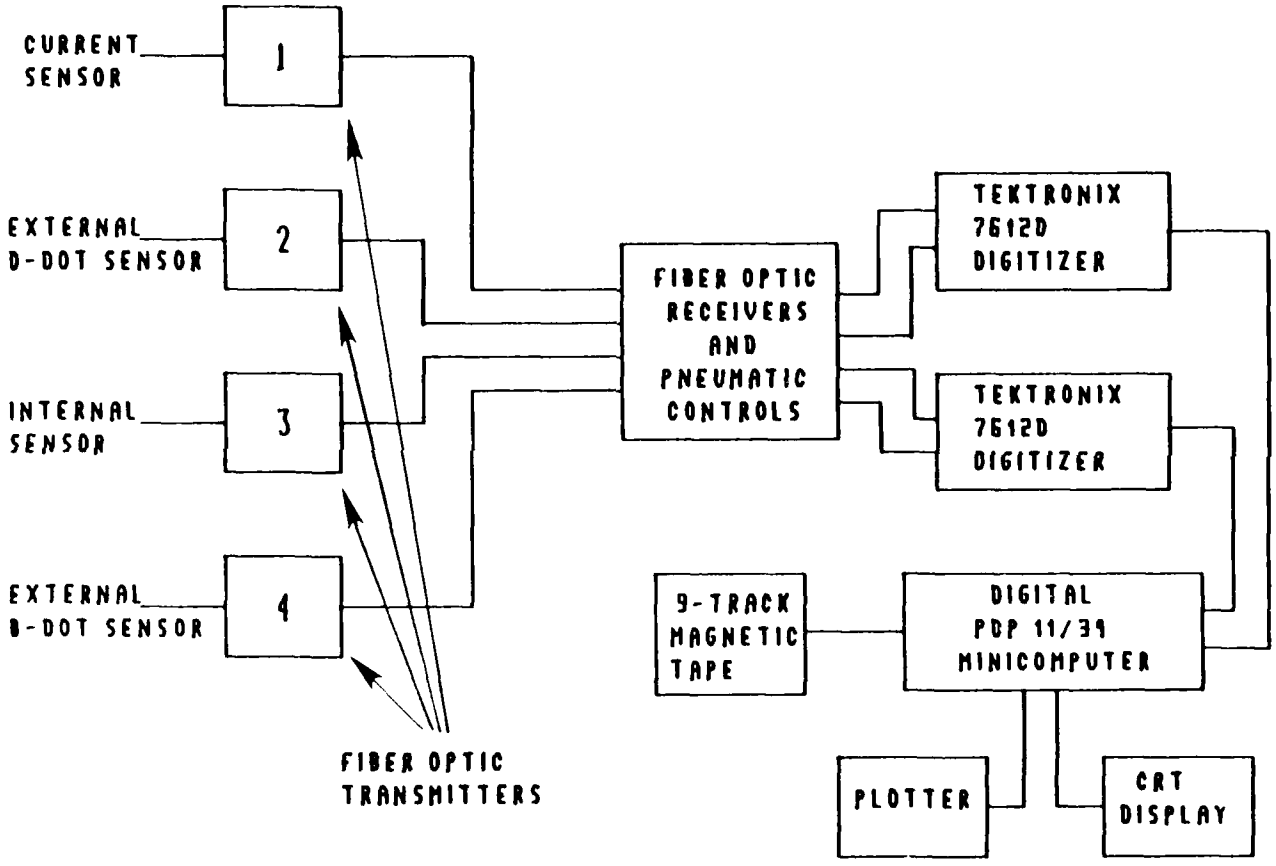


Figure 8. Block Diagram of Data Acquisition System.

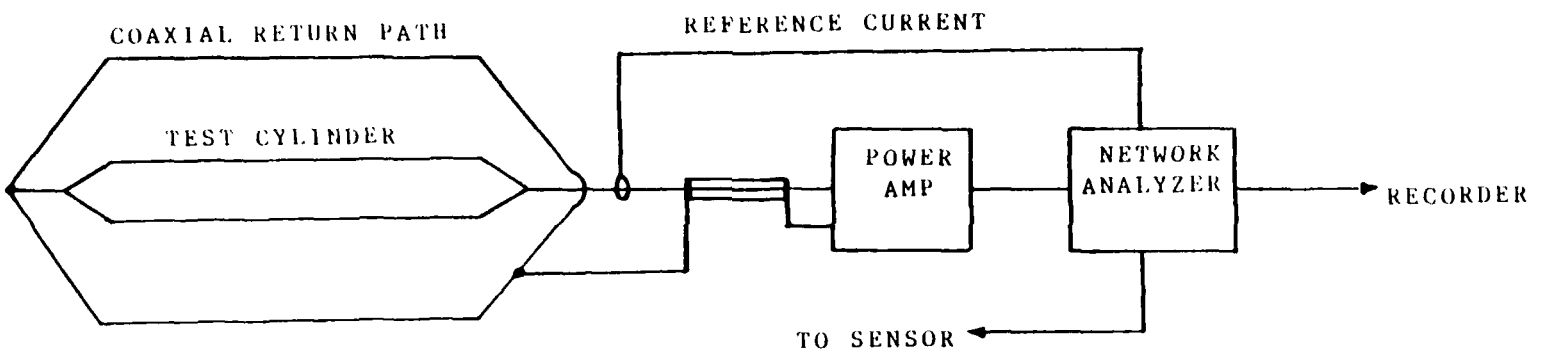


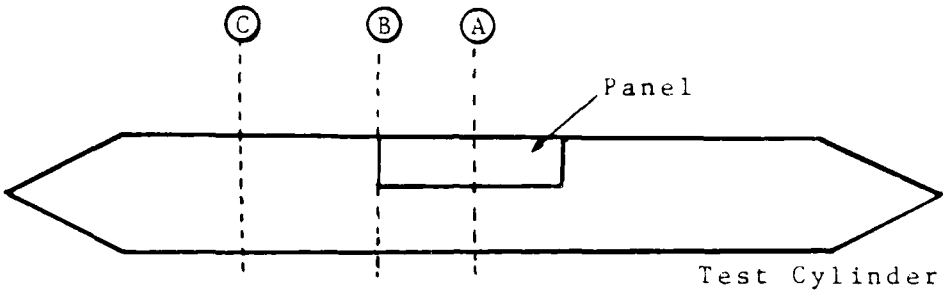
Figure 9. Swept Frequency CW Test Setup.

measure the magnetic field responses to the swept frequency CW induced currents. The sensor responses are fed back into the network analyzer. Through fiber optic links, the response and the input current are recorded by the Digital PDP 11/34 computer and stored on magnetic disks. The locations of the sensor measurements used in this thesis are depicted in Figure 10. The SFCW tests were conducted on the cylinder with the open aperture, the solid aluminum panel, the composite #1 panel, and the composite #2 panel.

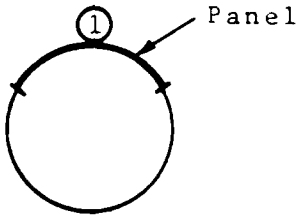
Current Pulse Measurements

The second part of the experimental measurements were made using the current pulse lightning simulation technique. The Lightning Test Cylinder was configured with the coaxial return path, which is identical to the swept frequency CW setup except for the 50 ohm load between the cylinder and coaxial return. The setup for the current pulse measurement is illustrated in Figure 11.

The current pulse is produced by a generator consisting of two banks of capacitors, each with a capacitance of eight microfarads. Each capacitor bank can be charged to 100kV resulting in a 200 kV potential difference capability for the current pulse generator. For this thesis, three different current pulse waveforms were injected into the cylinder. The first type of current pulse was a unipolar, double-exponential waveform with a 20 kA current peak. A typical unipolar waveform that was used in the testing is



SIDE VIEW



CROSS SECTION

B-Dot Sensor Locations

A1

B1

C1

Figure 10. Sensor Locations for SFCW Test.

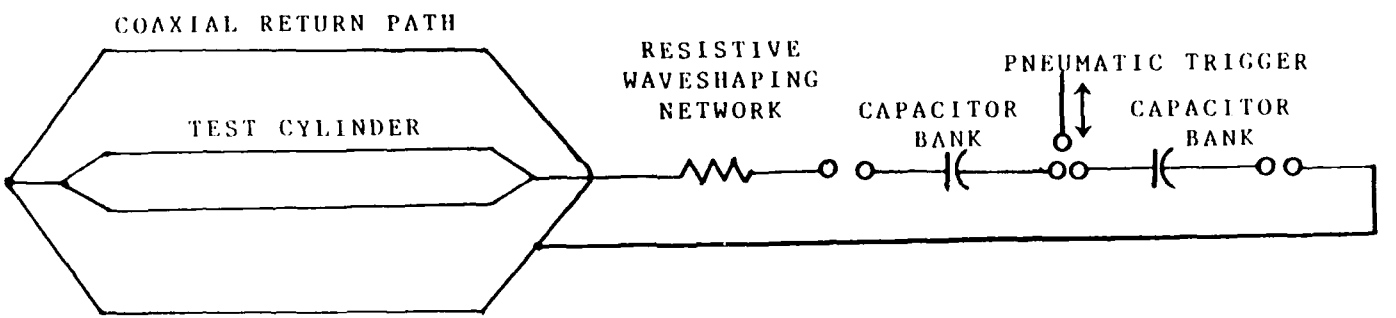


Figure 11. Current Pulse Test Setup.

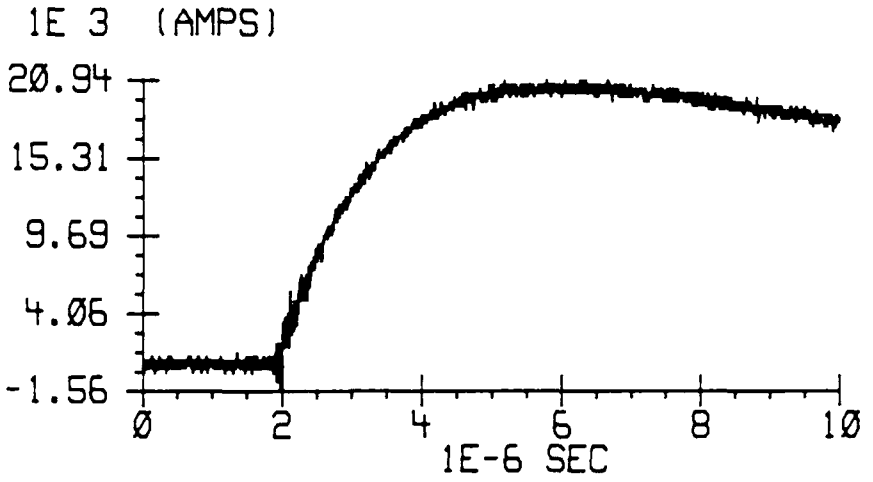


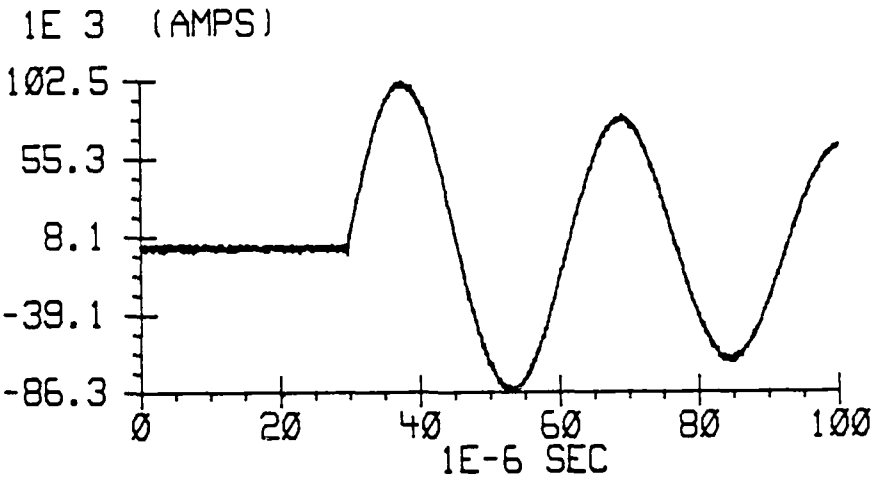
Figure 12. Unipolar, Double-Exponential 20kA Current Pulse.

depicted in Figure 12. The overdamped unipolar, RLC-type, double-exponential waveshape is achieved by inserting a resistive network with a total impedance of 5.5 ohms into the test configuration.

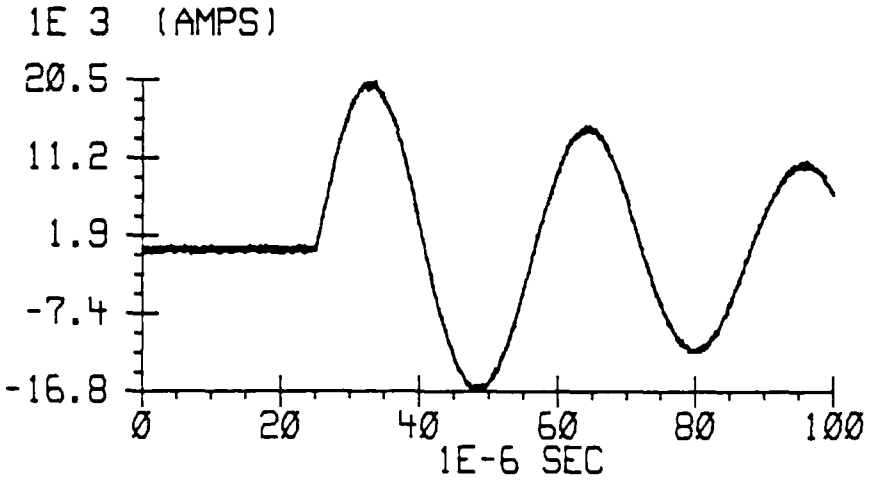
The other two types of current pulses injected into the cylinder are oscillatory waveforms. In order to attain higher current levels with the current pulse technique, it is necessary to remove the overdamping resistive waveshaping network from the setup circuit. With the resistive network removed, a damped oscillatory current waveform with a peak

amplitude of 100 kA is injected into the cylinder. Figure 13a illustrates a typical oscillatory waveform for a 100 microsecond window. An oscillatory current waveform with a peak amplitude of 20 kA, shown in Figure 13b, was also injected into the cylinder for comparison with results from the unipolar, double-exponential current pulse with the 20 kA peak.

The current pulse was measured with a T&M current transformer located at the rear of the cylinder. The current transformer has a load of 0.005 ohms. External and internal field measurements of the cylinder were also taken. The internal sensors used during the current injection tests were EG&G hollow spherical dipole (HSD) D-dot sensors for electric field measurements and EG&G cylindrical moebius loop (CML) B-dot sensors for magnetic field measurements. External magnetic field measurements for the unipolar 20 kA current pulse tests were also performed by CML B-dot sensors. External magnetic field measurements for the oscillatory current waveforms were done by multi-gap loop (MGL) B-dot sensors. Asymptotic conical dipole (ACD) D-dot sensors were utilized for external electric field measurements. Figure 14 depicts the locations of the D-dot and B-dot sensors on the cylinder where measurements were recorded during the current pulse tests. The current pulse tests were conducted with the aperture open, or covered by the solid aluminum, the composite #1, and the composite #2

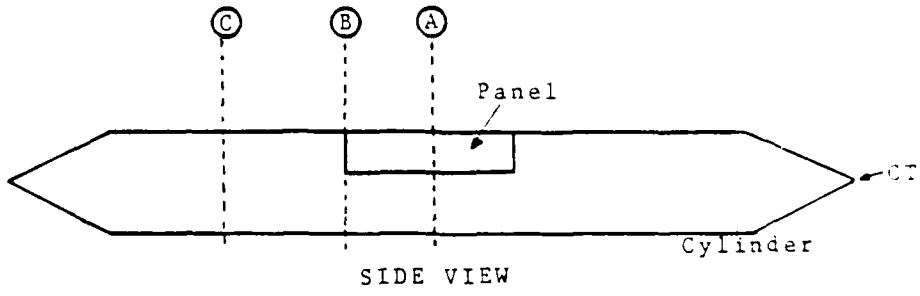


[a]

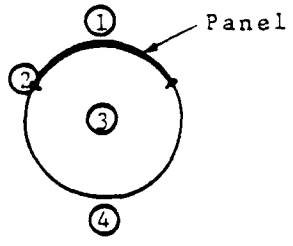


[b]

Figure 13. Oscillatory Current Waveforms: (a) 100 kA Peak and (b) 20 kA Peak.



SIDE VIEW



CROSS SECTION

Sensor Locations

D-dot	B-dot
A1	A1
A2	A2
A3	A3
A4	A4
B1	B1
B2	B2
B3	B3
B4	B4
	C1
	C4

Figure 14. Sensor Locations for Current Pulse Test.

panels using the 20 kA unipolar, 20 kA oscillatory, and 100 kA oscillatory injected waveforms.

Shock-Excitation Measurements

The final lightning simulation test that was conducted on the cylinder incorporated the shock-excitation technique. The test setup is depicted in Figure 15, where a flat ground plate, rather than a coaxial, return path was used in the configuration. The cylinder was supported 75 centimeters above the ground plate by two dielectric stands.

The excitation source is provided by a Marx generator. The Marx generator used in this shock-excitation configuration consists of 29 stages of 0.7 microfarads capacitors. Each capacitor can be charged to 50 kV which results in a total discharge voltage potential of about 1.45 megavolts. For the shock-excitation measurements in this thesis, the Marx generator was charged to deliver one megavolt. The waveshaping network on the discharge end of the Marx generator consists of a total resistance of 1800 ohms in series with an inductor of 116 microhenries. A grounded electrostatic shield is placed between the Marx generator and the test cylinder in order to shield the cylinder from the fields generated by the Marx as it discharges.

The input and output spark gaps were separated at various distances to examine its effects on charging and discharging transients on the cylinder. Input spark gaps of

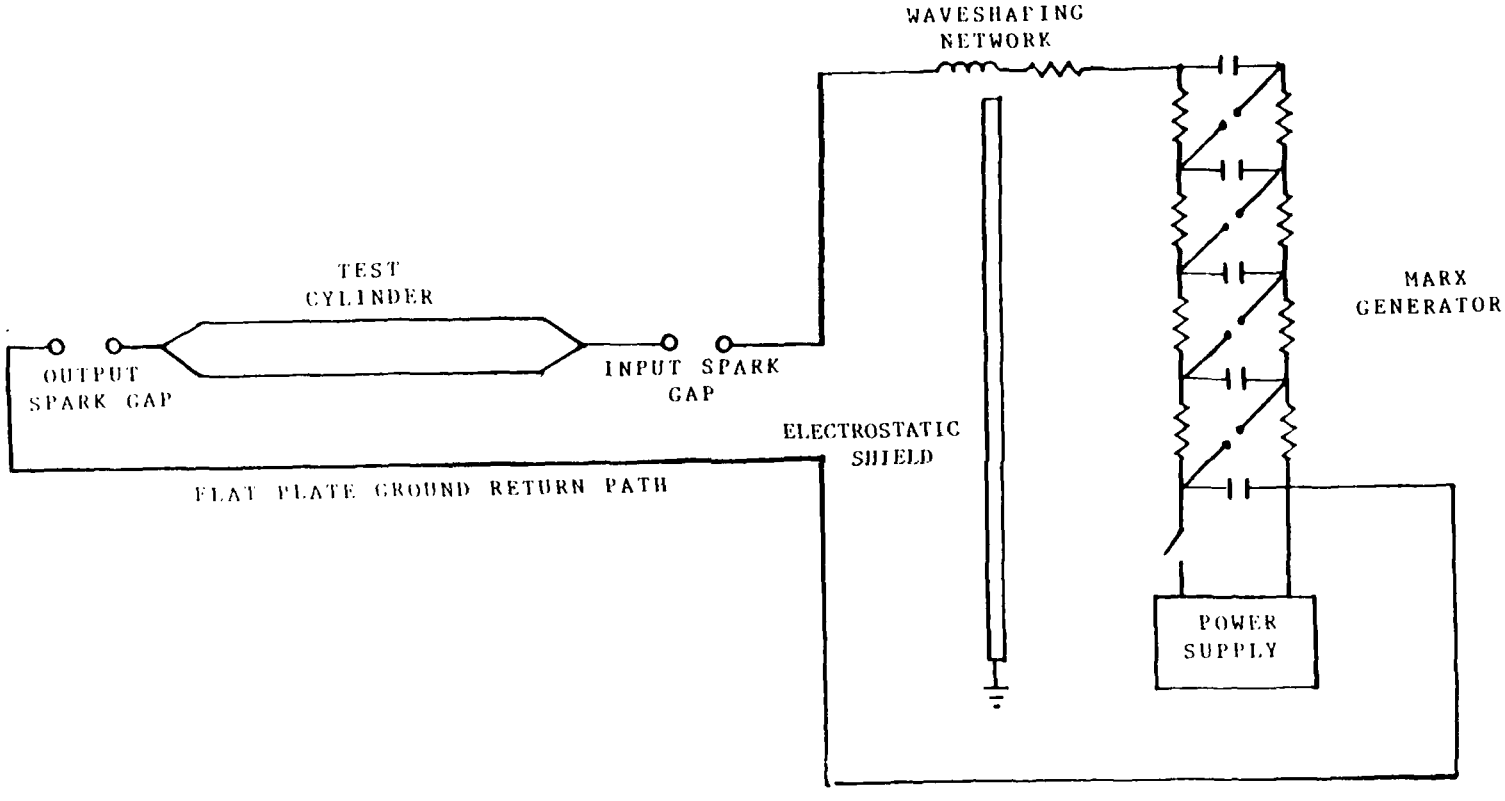


Figure 15. Shock-Excitation Test Setup.

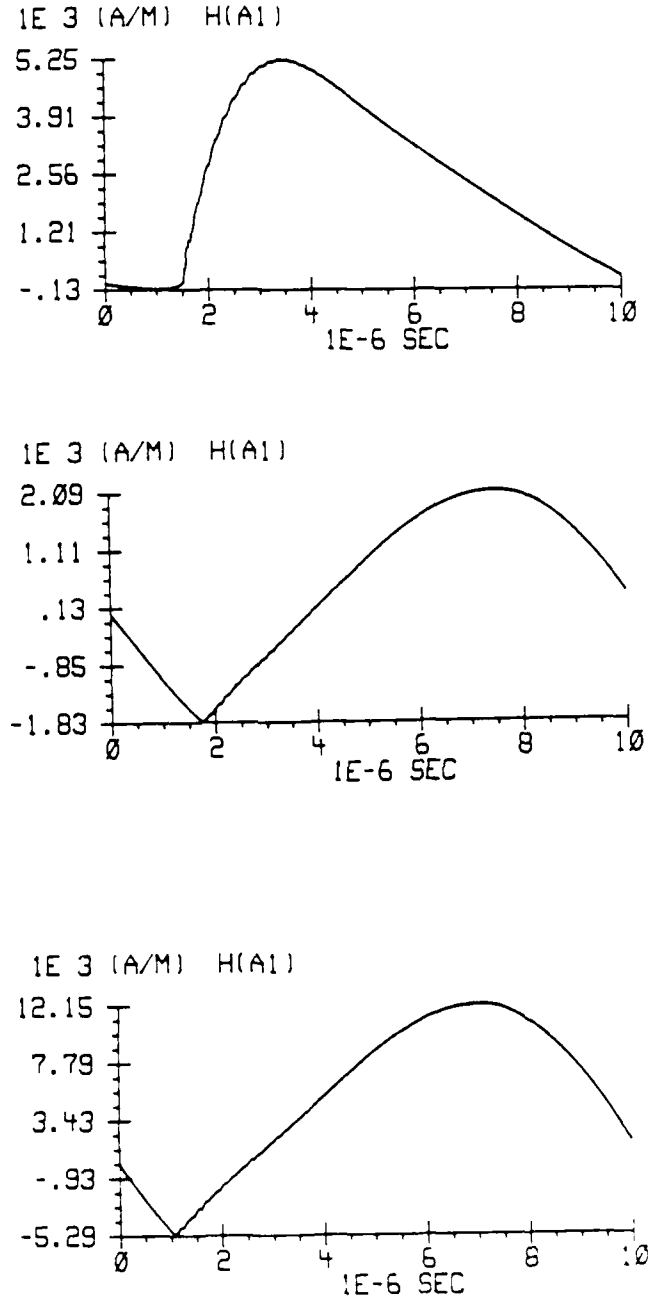


Figure 25. P3 External H-Field Responses for Current Pulse: *(a) 20 kA Unipolar, (b) 20 kA Oscillatory, and (c) 100 kA* Oscillatory.

electric field as the current is injected into the cylinder. However, the positive field following the negative electric field, which is seen in the unipolar results, is not apparent in the external responses of the 20 kA and 100 kA oscillatory currents. The electric field responses oscillate in the negative region for almost the entire 10.24 microsecond window.

The external magnetic field responses (Figure 25) tend to follow tne same waveshape as the corresponding injected current pulse -- unipolar and oscillatory. This is due to the direct proportional relationship from Ampere's law between the H-field and current for a cylindrical conductor. Although the injected excitation source is actually a negative current pulse, the H-field responses are plotted for convenience to indicate a positive current.

External Field Responses to Shock-Excitation

The shock-excitation responses presented in this section is for solid aluminum panel configuration using the 60 centimeter input spark gap and the 30 centimeter output spark gap setup. Figure 26 shows the external electric field response for the shock-excitation simulation. Note the initial, almost linear, negative increase in the electric field due to input spark gap breakdown, which is followed by charging phase of the simulation. Once the arc across the output spark gap has been established, the

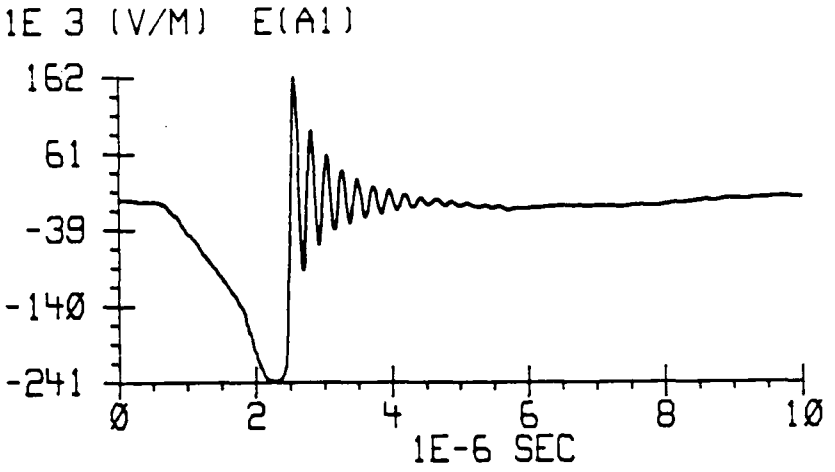


Figure 26. P3 External E-Field Response for Shock-Excitation.

electric field immediately oscillates with the excitation current flowing through the cylinder.

The external H-field response is illustrated in Figure 27. During the input spark gap breakdown and the charging phase of the shock-excitation simulation, the H-field has a negative rate of change. The H-field then experiences a very rapid positive change once the output arc has been established. Similar to the E-field response, the H-field then follows the excitation source as the oscillating current is discharged through the cylinder.

Comparison of Transfer Functions

This section will discuss the comparisons between the transfer functions that were derived from the SFCW, current

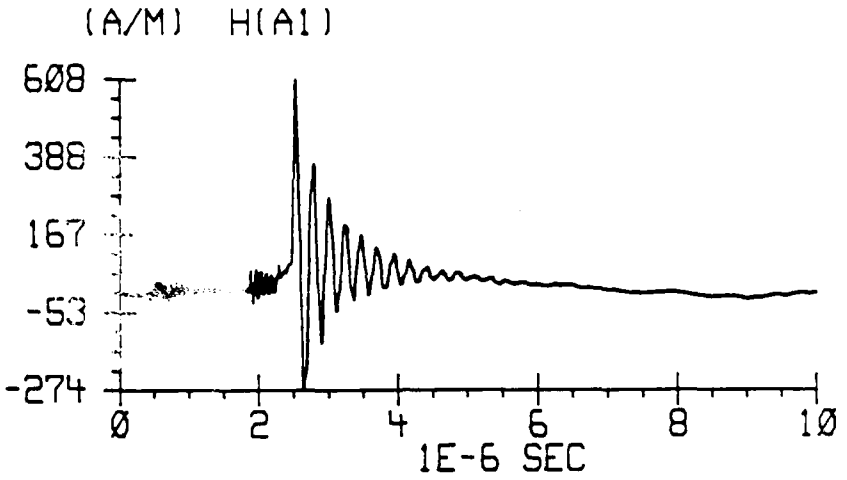
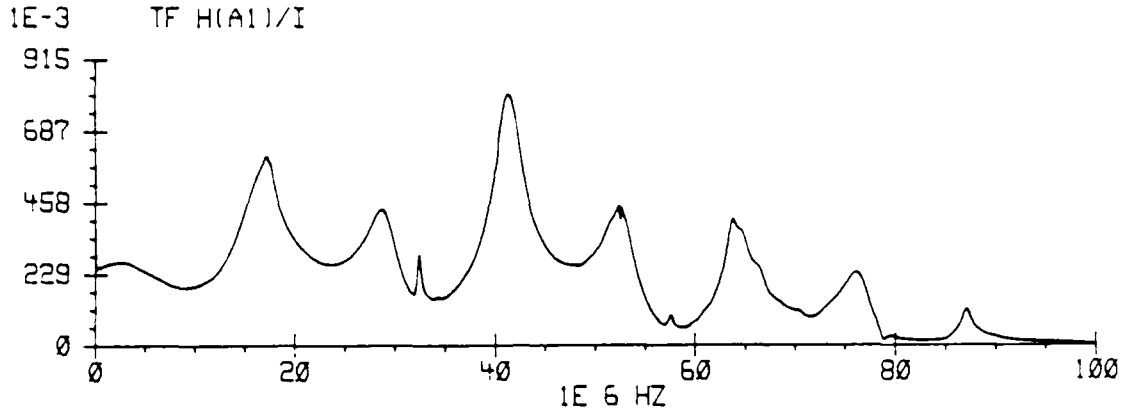


Figure 27. P3 External H-Field Response for Shock-Excitation.

pulse, and shock-excitation lightning simulation techniques. Figure 28 depict the transfer function of the external H-field determined by the SFCW technique for the P3 setup. A corresponding linear plot of the transfer function is also shown in order to clearly identify particular frequencies. The SFCW derived transfer functions are first compared to those obtained from the current pulse tests, which are shown in Figures 29 through 31, for the external H-field responses. In the case of the current pulse technique, one notes the decreasing magnitude of the transfer functions of the external magnetic field response to the excitation current at higher frequencies. This general trend is seen for both the unipolar current pulse (Figure 29) and



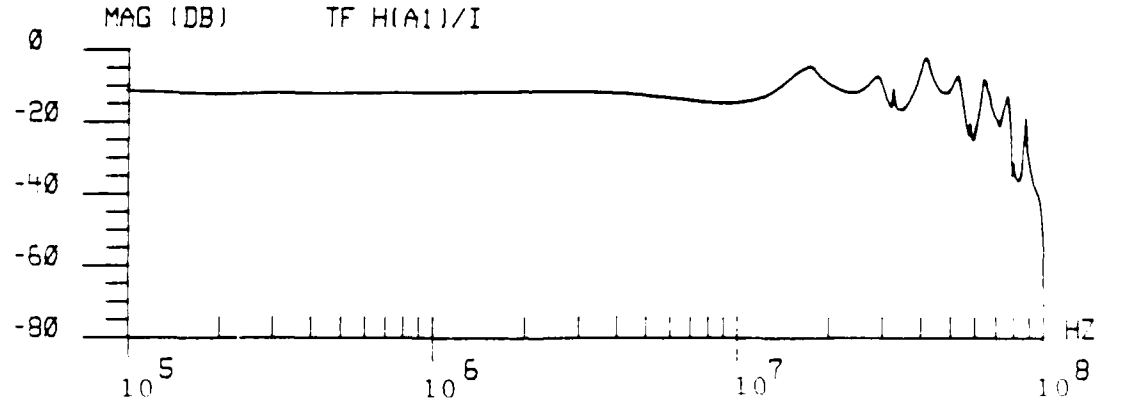
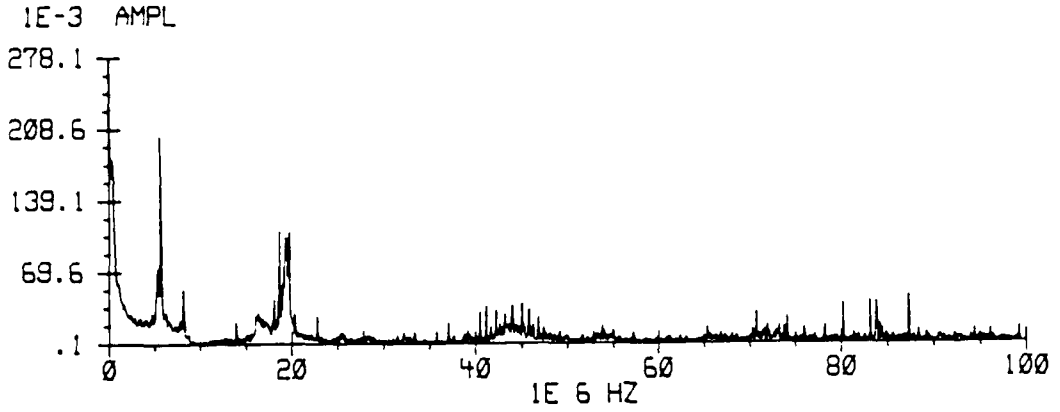


Figure 28. P3 External H-Field Transfer Function for SFCW.



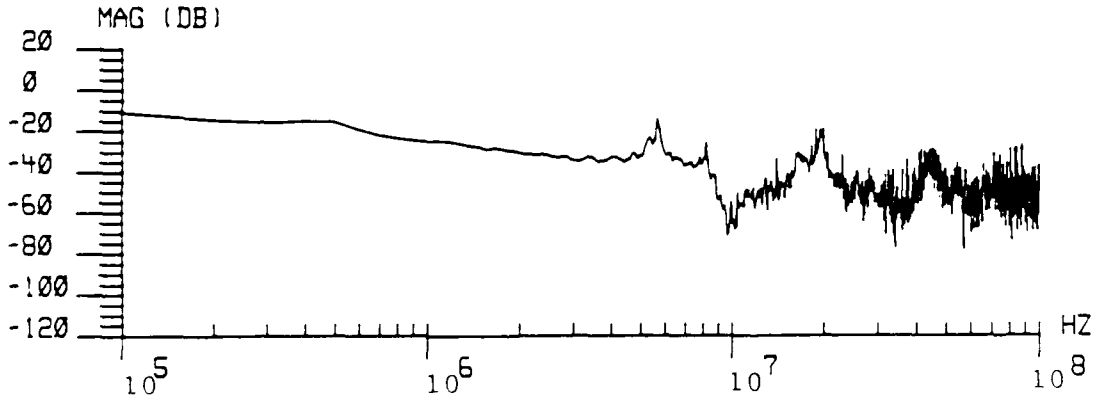
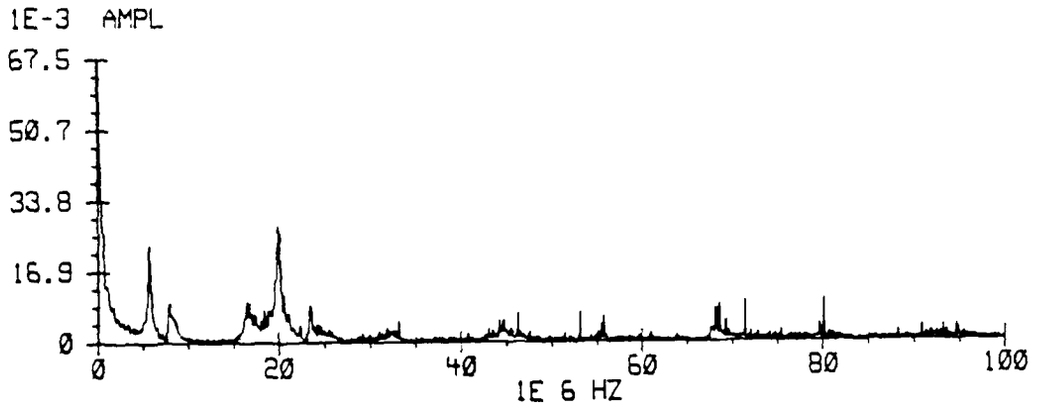


Figure 29. P3 External H-Field Transfer Function for 20 kA Unipolar Current Pulse.



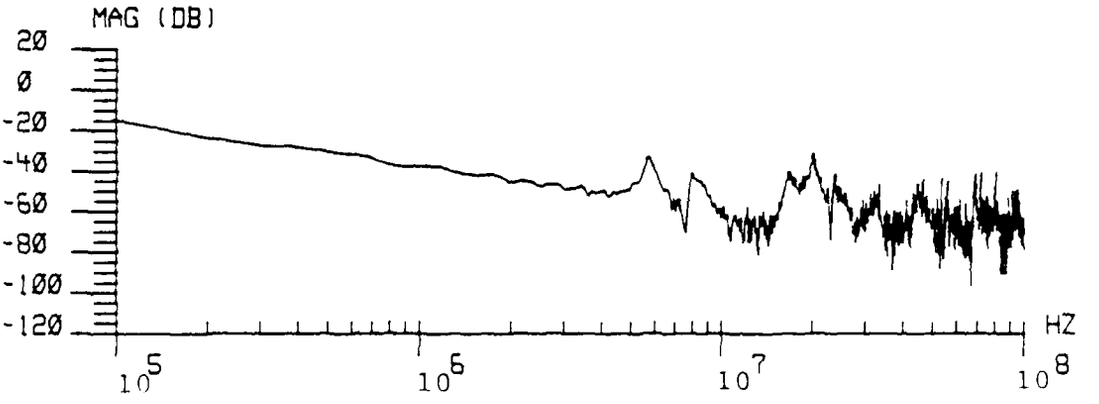
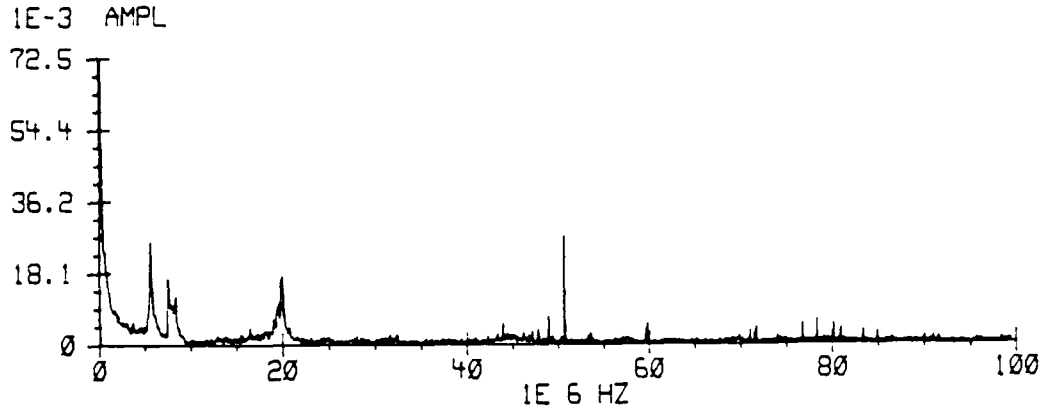


Figure 30. P3 External H-Field Transfer Function for 20 kA Oscillatory Current Pulse.



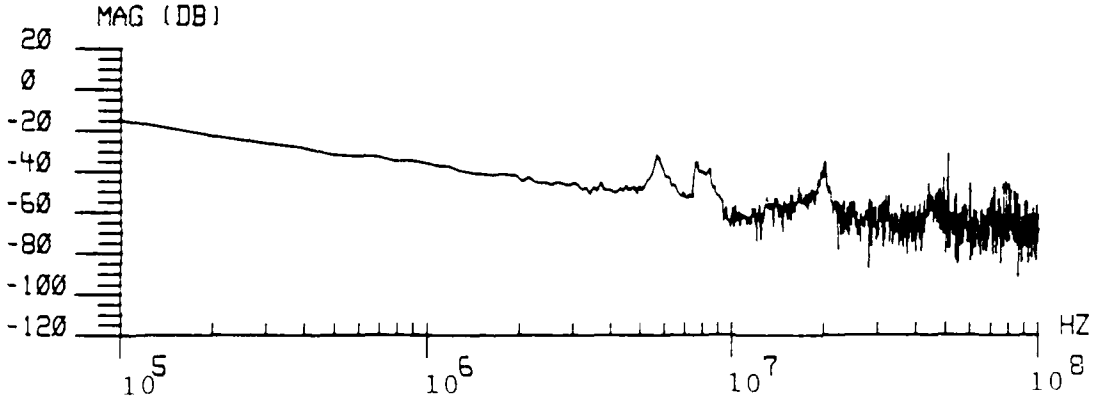
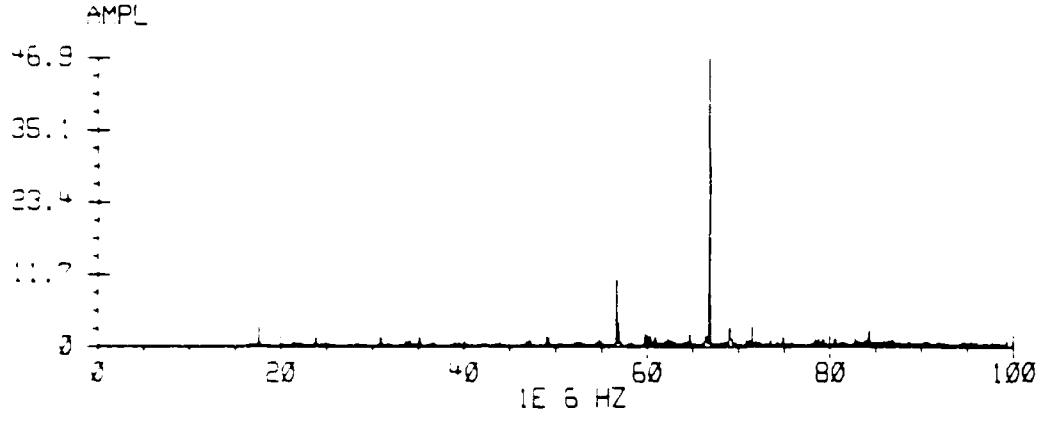


Figure 31. P3 External H-Field Transfer Function for 100 kA Oscillatory Current Pulse.

oscillatory current pulse results (Figures 30 and 31). This is unlike the transfer functions obtained from the SFCW technique which have a relatively constant magnitude until about 80 MHz. The oscillatory transfer functions, 20 kA and 100 kA, have a faster decrease in magnitude with increasing frequency, however, when compared to the unipolar case. The differences between the transfer functions of the various simulation techniques are also seen when they are compared to those of the shock-excitation technique. Figure 32 shows the external magnetic field transfer function that is derived with respect to the excitation current. For the shock-excitation case, the transfer function tend to increase in magnitude at higher frequencies. This effect is possibly due to the very fast risetimes of the excitation current that are obtained with the shock-excitation technique.

The linear plots of the transfer functions clearly identify specific lobes. In Figure 28, spikes in the transfer function occur at 17, 29, 41, 52, 64, and 87 MHz for the SFCW case. The most prominent lobe appears at 41 MHz for the solid aluminum panel configuration P3.

The external H-field transfer functions for the current pulse case (Figures 29 through 31) indicate lobes at 6, 8, 17, and 20 MHz, in addition to a number of lobes between 40 to 60 MHz, for both the unipolar and the oscillatory current pulses. Those lobes occuring at 17 MHz and between the 40



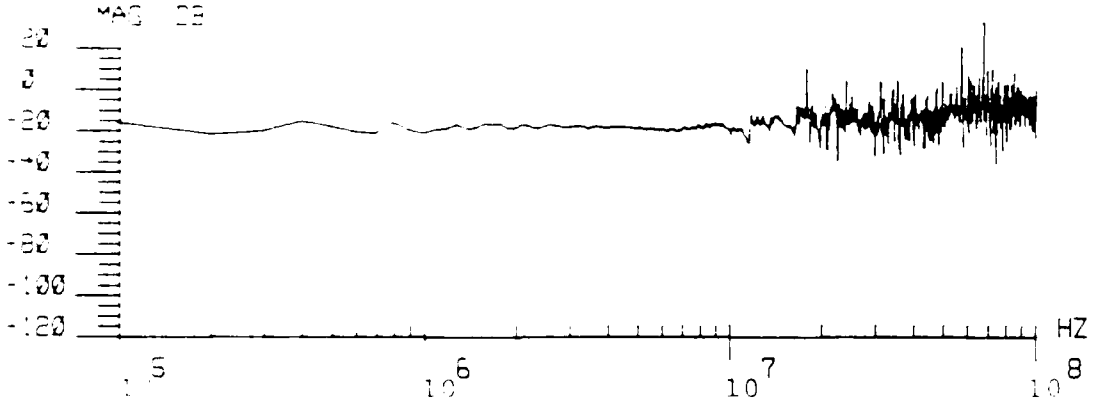


Figure 32. P3 External H-Field Transfer Function for Shock-Excitation.

to 60 MHz bandwidth can be correlated to lobes at the same frequencies for the SFCW derived transfer function.

The external H-field transfer function for the shock-excitation setup (Figure 32) shows very large spikes at 57 and 67 MHz. These characteristic lobes are possibly due to the facility effects such as the return path and the generator used during the shock-excitation tests.

The external E-field transfer functions resulting from the current pulse measurements are illustrated in Figures 33 through 35. These transfer functions show a relatively constant magnitude until the first large lobe occuring at 6 MHz. All of the transfer functions then decrease in magnitude for frequencies beyond 6 MHz. Unlike the transfer function of the 20 kA unipolar (Figure 33) and the 100 kA oscillatory (Figure 35) current pulses, the transfer function of the 20 kA oscillatory pulse (Figure 34) experiences a number of nulls prior to the 6 MHz mark. However, in all cases, unipolar and oscillatory, another lobe is present at 8 MHz that is soon followed by nulls at 10 and 16 MHz. Other lobes occur at 13, 17, and 20 MHz.

The shock-excitation transfer function of the external electric field is depicted in Figure 36 for the solid aluminum panel configuration. As the frequency increases, the magnitude of the transfer functions also increase until the first relative null at approximately 600 kHz. The magnitude then decreases as the frequency approaches 12 MHz.

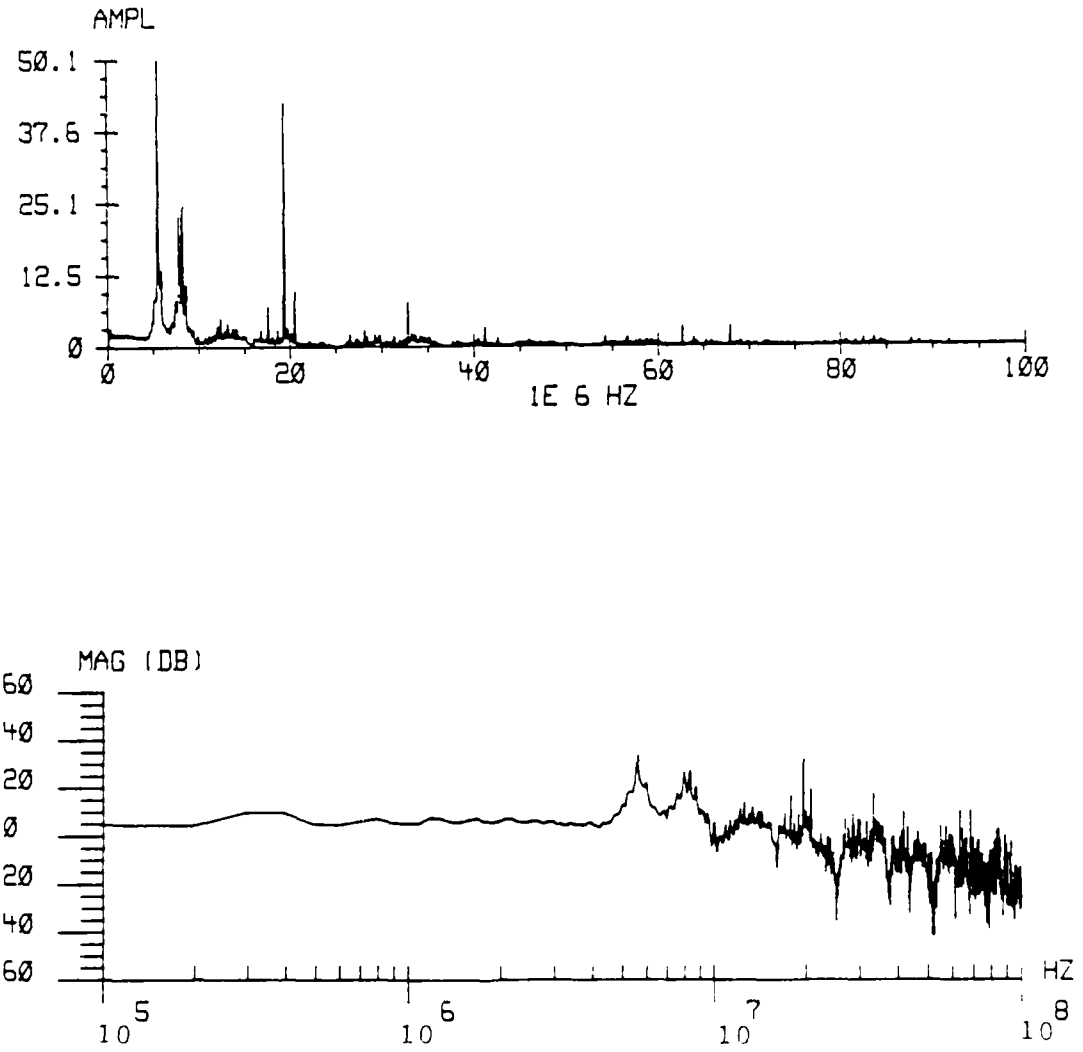
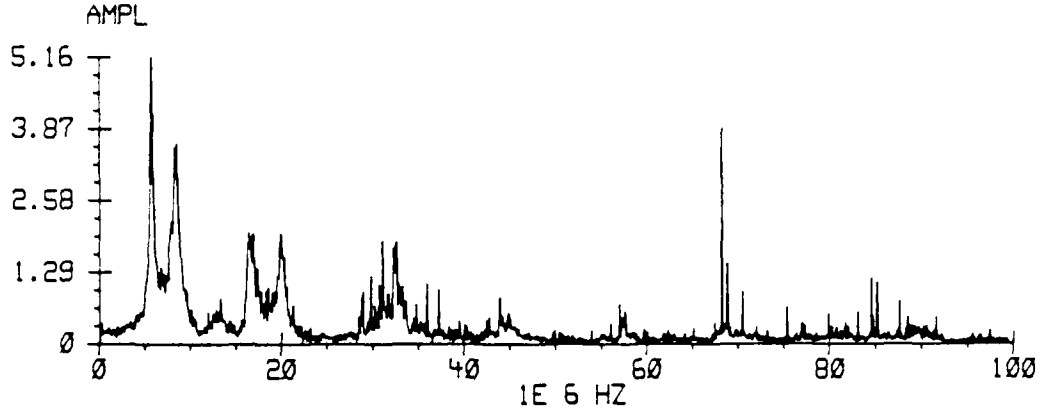


Figure 33. P3 External E-Field Transfer Function for 20 kA Unipolar Current Pulse.



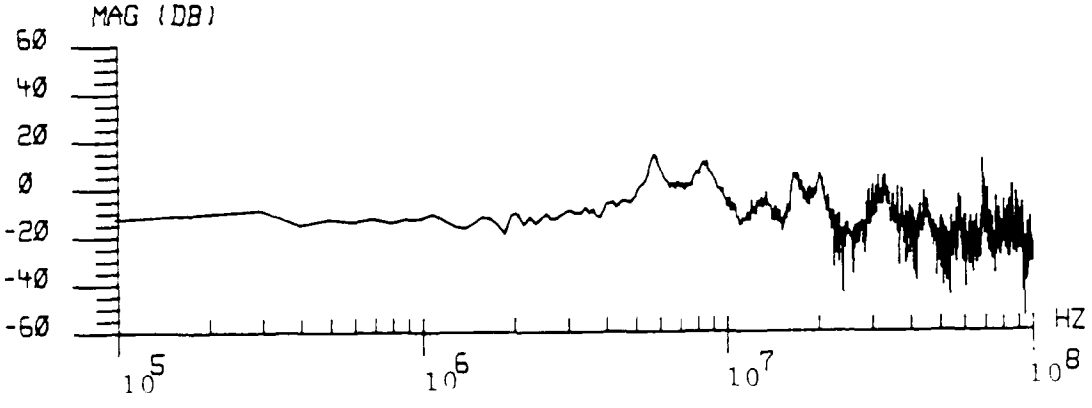
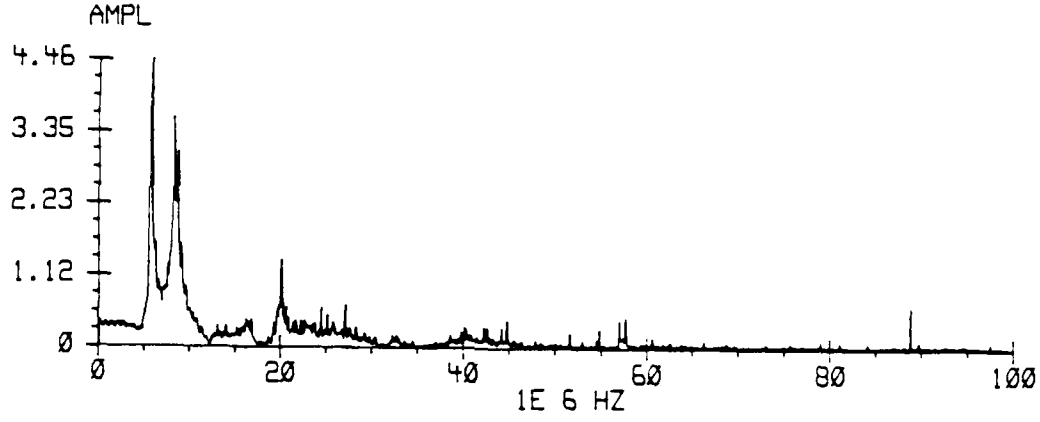


Figure 34. P3 External E-Field Transfer Function for 20 kA Oscillatory Current Pulse.



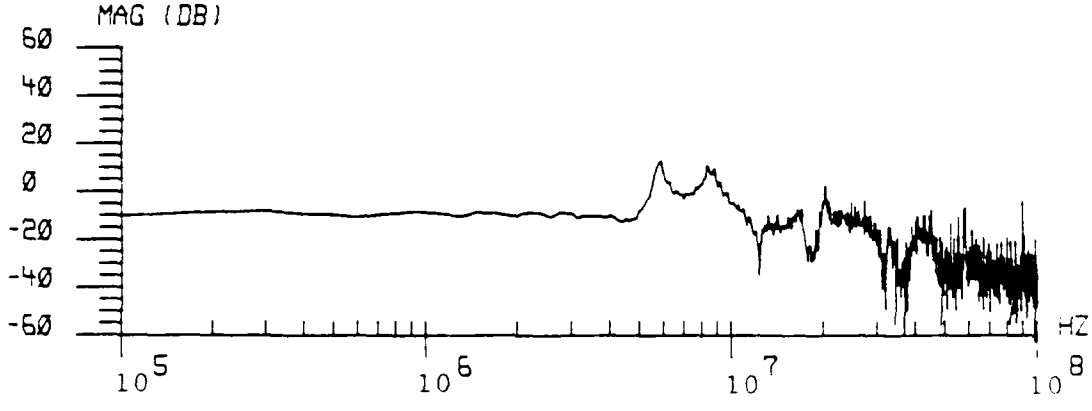
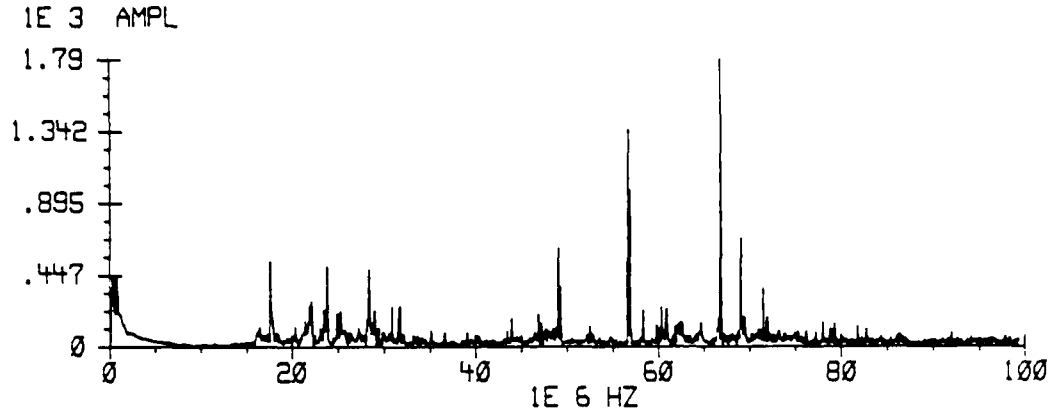


Figure 35. P3 External E-Field Transfer Function for 100 kA Oscillatory Current Pulse.



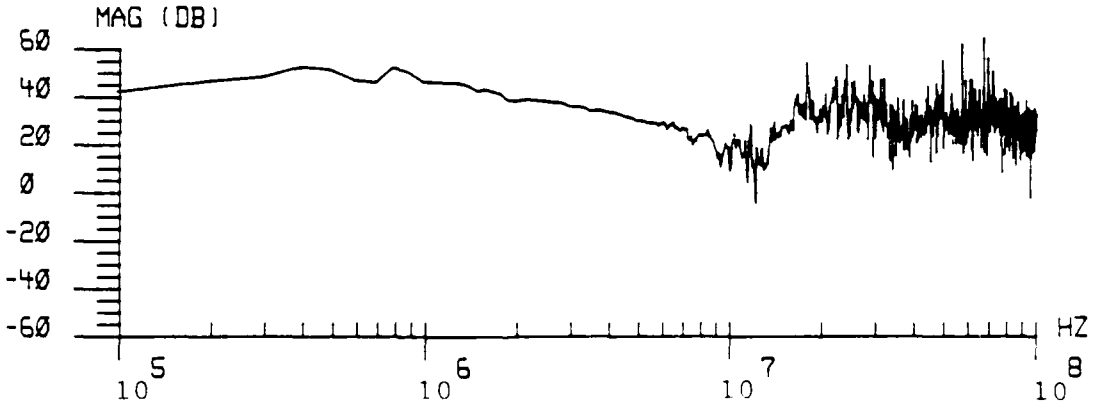


Figure 36. P3 External E-Field Transfer Function for Shock-Excitation.

The shock-excitation transfer function of the external E-field has characteristic lobes at 400 and 800 kHz and a null at 12 MHz. At the higher frequencies, prominent spikes appear at 57, 69, and 72 MHz, as well as the extremely large lobe at 67 MHz. Those spikes appearing at 57 and 67 MHz also occur in the shock-excitation transfer function for the external H-field (Figure 32). Again, these two spikes may be an effect resulting from the facility setup of the shock-excitation simulation; specifically, the flat ground plate return path and the Marx generator.

Threat-Level Field Responses

Since the transfer functions that were derived for each of the various simulation techniques uniquely describe the induced electric and magnetic fields on the test cylinder, the threat-level field responses can be predicted. Using the assumption that the electromagnetic interaction is a linear process, the threat-level field responses are determined by folding the threat-level current waveform into the transfer function. The threat waveform used in this thesis for response prediction is the Current Waveform Component A, which represents the severe case of a first return stroke. This double exponential waveform has a peak amplitude of 200 kA and an action integral of 2×10^2 A^2s.

The current waveform is mathematically defined as

$$i(t) = I_o \left[e^{-at} - e^{-bt} \right] \qquad (19)$$

where

I_o = 218,810 (A)

a = 11,354 (sec^{-1})

b = 647,265 (sec^{-1})

t = time (sec)

The waveform is illustrated in Figure 37.

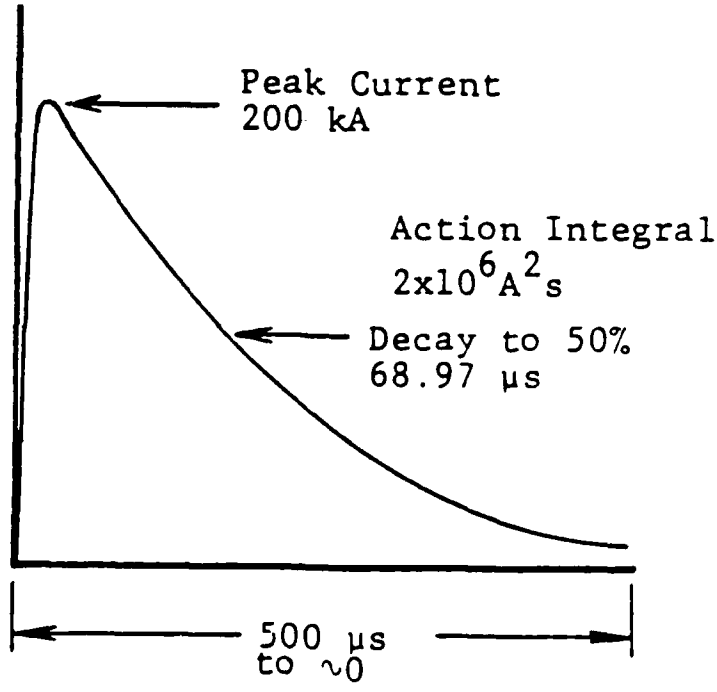


Figure 37. Full Threat-Level Current Waveform Component A.

The peak response values of the predicted full threat-level electric field and magnetic field are shown in Table 1. Both external (Location A1) and internal (Location A3) field responses were computed for the various panel configurations and lightning simulation techniques. Since the transfer functions derived from the SFCW technique were determined only for the external H-field, the SFCW threat-level predictions do not include the internal and external E-field responses and the internal H-field responses.

In comparing the full threat-level responses, the results of the solid panel configuration are used. The peak external H-field responses for the different simulation techniques are graphically illustrated in Figure 38. The SFCW technique has the largest threat-level response with a predicted peak value of 58.3 kA/m. This is about twice the peak H-field response values predicted by the shock-excitation technique and the 20 kA unipolar current pulse technique. The two smallest predicted values are given by both oscillatory current pulse methods.

Figure 39 is a graphical presentation of the peak external E-field responses to the threat current waveform. The magnitude of the peak electric field response predicted by the shock-excitation technique is over 100 times the peak response values predicted by the unipolar and oscillatory current pulse techniques. The shock-excitation E-field peak

Table 1.

Responses to Threat-Level Current Waveform

Test	Field	P0	P1	P2	P3
SFCW	H(A1) [A/m]	31.2E3	52.6E3	62.1E3	58.3E3
C20u	H(A1) [A/m]	14.1E3	26.6E3	27.2E3	26.0E3
C20o	H(A1) [A/m]	5.7E3	17.3E3	20.8E3	10.2E3
C100o	H(A1) [A/m]	3.7E3	10.8E3	12.6E3	11.4E3
SE	H(A1) [A/m]	121.3E3	35.5E3	32.2E3	31.5E3
C20u	E(A1) [V/m]	496E3	431E3	537E3	485E3
C20o	E(A1) [V/m]	86E3	37E3	87E3	117E3
C100o	E(A1) [V/m]	76E3	71E3	89E3	117E3
SE	E(A1) [V/m]	46.9E6	45.6E6	52.9E6	49.7E6
C20u	H(A3) [A/m]	6.6E3	496	343	2.3
C20o	H(A3) [A/m]	3.2E3	432	217	1.1
C100o	H(A3) [A/m]	2.3E3	400	226	0.4
SE	H(A3) [A/m]	21.1E3	916	321	31.1
C20u	E(A3) [V/m]	443E3	14E3	6E3	3E3
C20o	E(A3) [V/m]	61E3	21E3	14E3	3E3
C100o	E(A3) [V/m]	74E3	18E3	9E3	1E3
'E	E(A3) [V/m]	26.9E6	71E3	43E3	57E3

Notation:
SFCW = swept frequency continuous wave
C20u = 20 kA unipolar current pulse
C20o = 20 kA oscillatory current pulse
C100o = 100 kA oscillatory current pulse
SE = shock-excitation
P0 = open aperture
P1 = composite #1 panel
P2 = composite #2 panel
P3 = solid aluminum panel

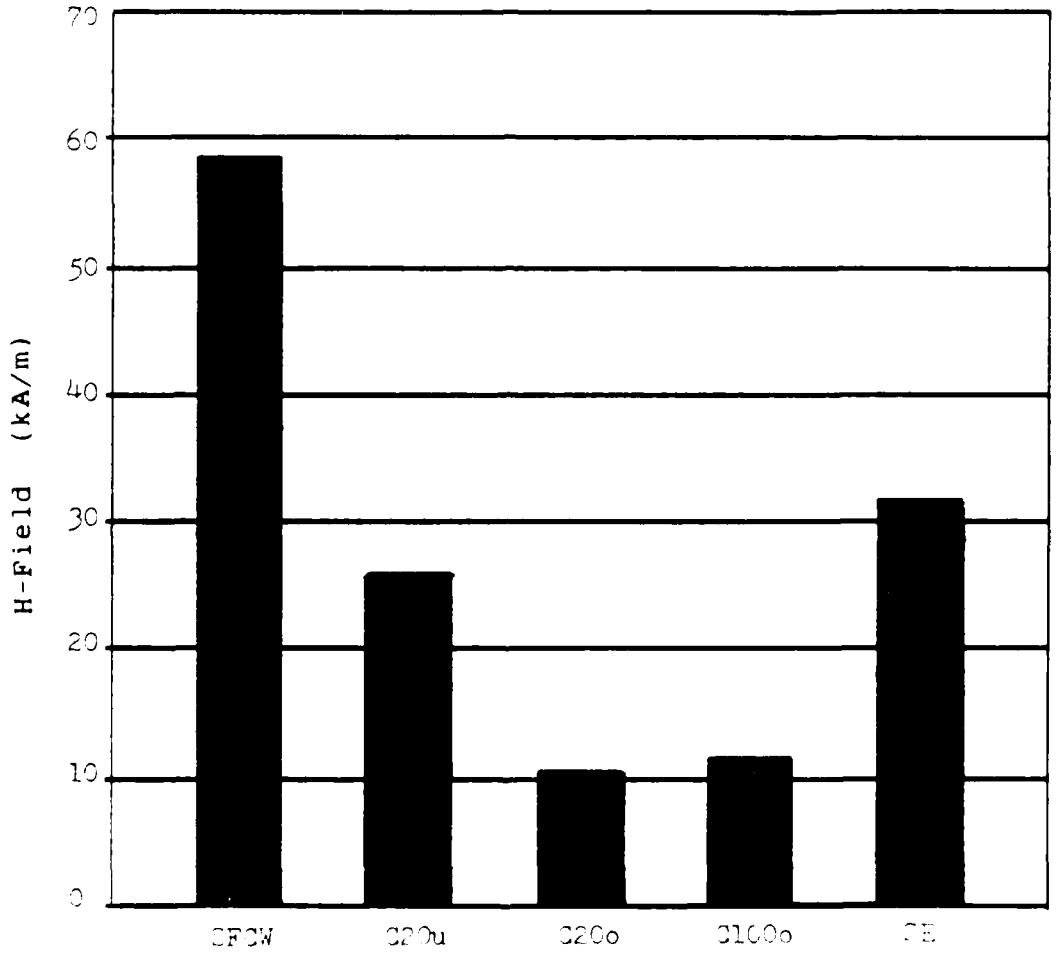


Figure 38. P3 Peak External H-Field Full Threat-Level Responses.

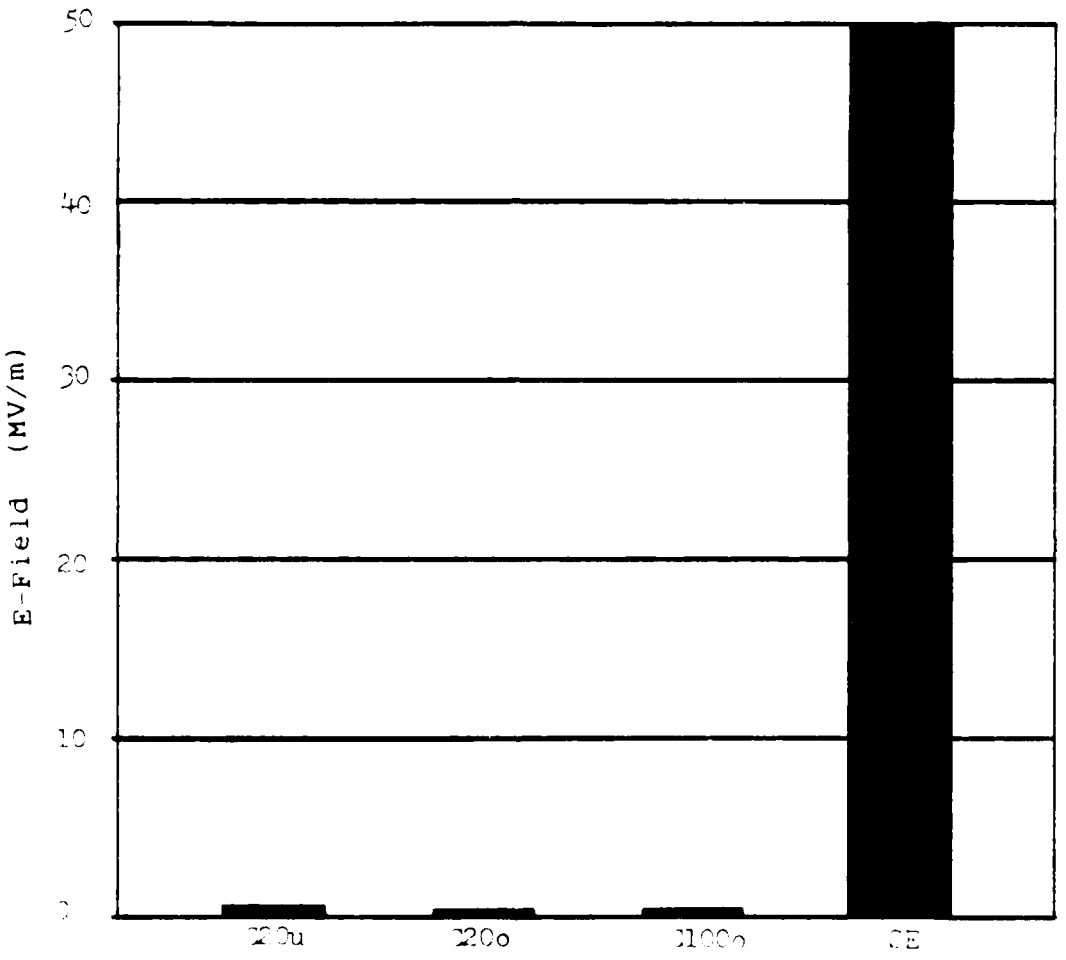


Figure 39. P3 Peak External E-Field Full Threat-Level Responses.

is 49.7 MV/m; whereas, the 20 kA unipolar current pulse response peak has a magnitude of 485 kV/m. As in the external H-field threat-level responses, the predictions by the two oscillatory current pulse methods have the smallest magnitudes of all of the test techniques. Both the 20 kA and the 100 kA oscillatory current pulse transfer functions compute an external E-field peak of 117 kV/m from the 200 kA threat current waveform.

The external H-field and E-field predictions are also extended to the internal field responses. The peak internal H-field and E-field responses to the threat current waveform are illustrated, respectively, in Figure 40 and Figure 41 for the solid aluminum panel configuration. In both cases, the peak internal field responses are dominated by the prediction generated by the shock-excitation simulation technique. The 20 kA unipolar case produces the largest internal H-field and E-field responses of the three current pulse techniques.

The predicted full threat-level responses can also be compared to the actual measured responses of the current pulse and the shock-excitation lightning simulation techniques. The measured peak magnetic and electric field responses for the various panel configurations are shown in Table 2. When compared to the predicted full threat-level responses shown in Table 1, one immediately observes that the actual measured peak field responses for the 100 kA

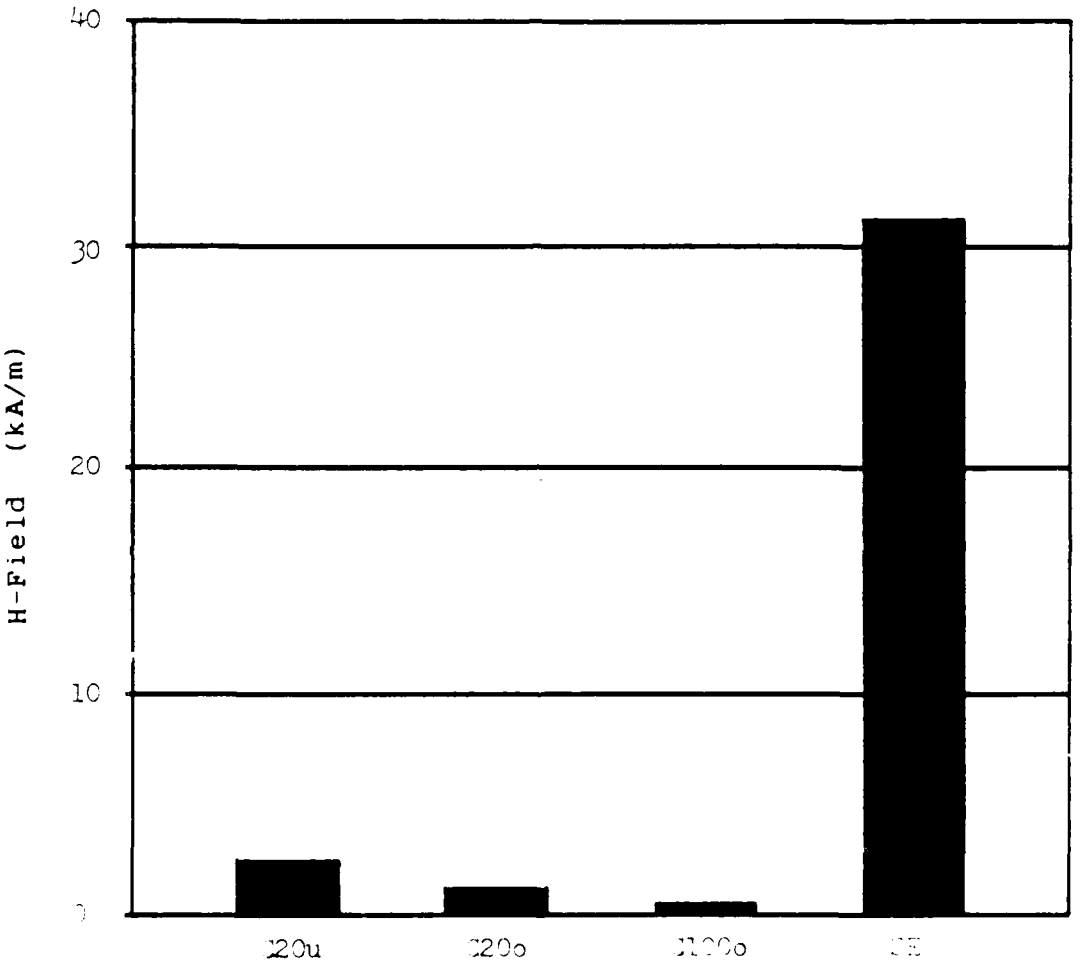


Figure 40. P3 Peak Internal H-Field Full Threat-Level Responses.

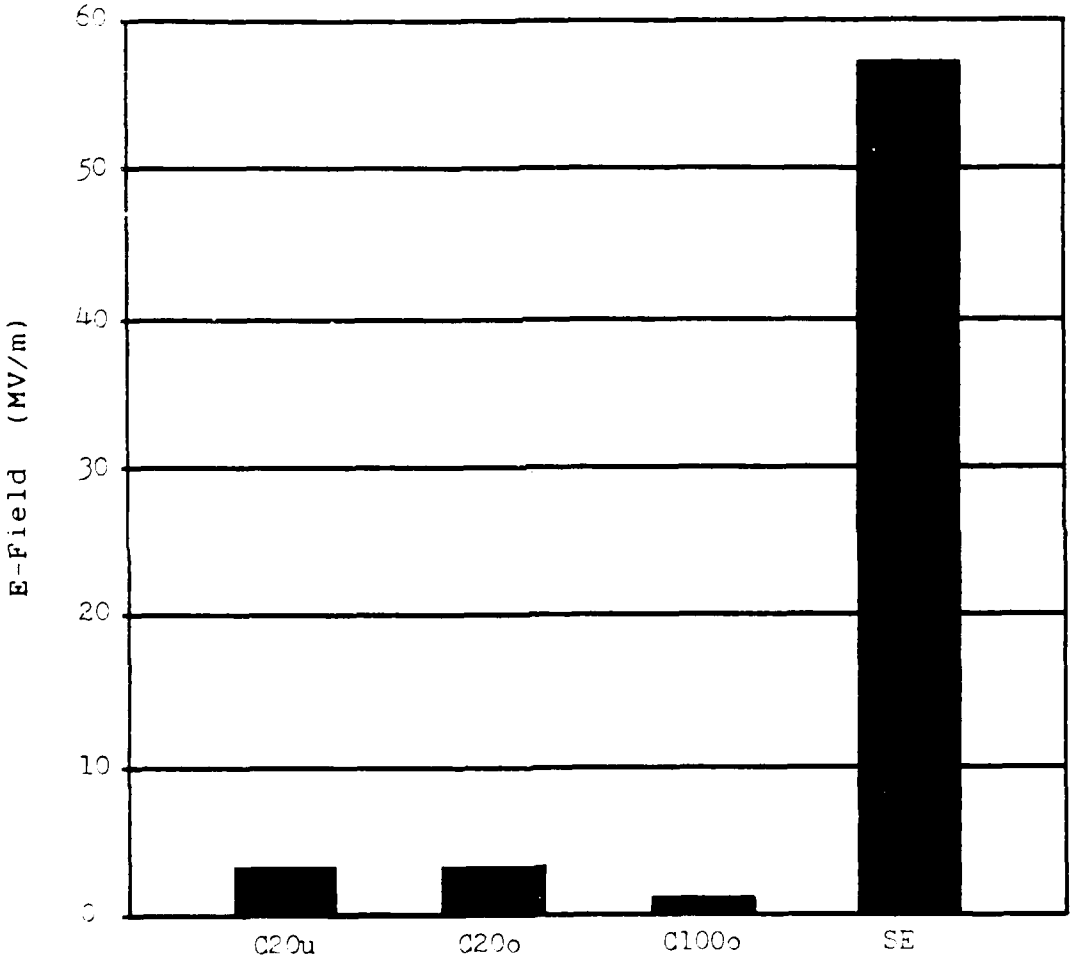


Figure 41. P3 Peak Internal E-Field Full Threat-Level Responses.

Table 2.

Measured Peak Field Responses

Test	Field	P0	P1	P2	P3
C20u	H(A1) [A/m]	2.9E3	5.2E3	5.3E3	5.3E3
C20o	H(A1) [A/m]	1.1E3	3.9E3	4.3E3	2.1E3
C100o	H(A1) [A/m]	3.1E3	11.7E3	13.0E3	12.2E3
SE	H(A1) [A/m]	400	603	592	608
C20u	E(A1) [V/m]	66.0E3	36.6E3	69.9E3	53.1E3
C20o	E(A1) [V/m]	10.1E3	5.9E3	9.1E3	14.2E3
C100o	E(A1) [V/m]	45.4E3	46.8E3	52.8E3	71.3E3
SE	E(A1) [V/m]	221E3	231E3	240E3	241E3
C20u	H(A3) [A/m]	1.4E3	123	80	0.5
C20o	H(A3) [A/m]	710	104	47	0.2
C100o	H(A3) [A/m]	3.0E3	503	278	0.5
SE	H(A3) [A/m]	410	4.9	2.1	0.1
C20u	E(A3) [V/m]	85.4E3	3.1E3	1.4E3	581
C20o	E(A3) [V/m]	14.4E3	5.5E3	2.8E3	470
C100o	E(A3) [V/m]	92.9E3	22.2E3	10.09E3	923
SE	E(A3) [V/m]	137.9E3	307	406	223

Notation:
SFCW = swept frequency continuous wave
C20u = 20 kA unipolar current pulse
C20o = 20 kA oscillatory current pulse
C100o = 100 kA oscillatory current pulse
SE = shock-excitation
P0 = open aperture
P1 = composite #1 panel
P2 = composite #2 panel
P3 = solid aluminum panel

oscillatory current pulse tests are very close to the corresponding predicted threat-level values. This observation appears to be true for all four panel configurations for both external and internal field responses -- magnetic and electric.

Comparisons to Airborne Data

In this section, the measured field responses and the transfer functions resulting from the current pulse and the shock-excitation simulation techniques are compared to measured lightning data from the lightning characterization program during 1984 and 1985. The maximum levels of electric and magnetic flux densities measured by the CV-580 aircraft during the two year program were 22 Coul/m^2/s and 3950 Wb/m^2/s, respectively (18:iv). Assuming that the relative permittivity and relative permeability are equal to one, this would correspond to an E-dot (dE/dt) of 3.7×10^{12} V/m/s and an H-dot (dH/dt) of 3.1×10^{9} A/m/s.

The peak E-dot and H-dot responses for the current pulse and shock-excitation techniques are shown in Table 3 for the solid aluminum panel configuration. As can be seen from this table, both the dE/dt's and dH/dt's generated by the current pulse and the shock-excitation techniques are very close to those measured in the airborne case. The peak H-dot responses achieved by both the current pulse and shock-excitation methods appear to be sufficient in simulating this airborne event parameter. However, it

Table 3.

Peak Time Rate-of-Change of External Field Responses Generated by Simulation Techniques for Solid Aluminum Panel Configuration

Test	Peak H-Dot(Al) [A/m/s]	Peak E-Dot(Al) [V/m/s]
C20u	10.6×10^9	1.2×10^{12}
C20o	3.8×10^9	0.7×10^{12}
C100o	12.6×10^9	1.2×10^{12}
SE	9.0×10^9	4.5×10^{12}
In-Flight	3.1×10^9	3.7×10^{12}

Notation:
C20u = 20 kA unipolar current pulse
C20o = 20 kA oscillatory current pulse
C100o = 100 kA oscillatory current pulse
SE = shock-excitation

appears that only the shock-excitation technique was able to generate the peak E-dot response that is sufficiently high enough to exceed the peak airborne measurement of 3.7 x 10 V/m/s. On the other hand, the peak E-dot responses produced by the unipolar and oscillatory current pulse methods are only several orders of magnitude below the transient produced by shock-excitation.

The external H-field transfer function for the airborne case, shown in Figure 42, is compared to the transfer functions obtained from the various simulation tests with the solid aluminum panel configuration. The major differences between the airborne and ground simulation transfer functions are the frequencies that correspond to dimensions of the CV-580 aircraft and the test cylinder, respectively. The spikes occuring at 4.7, 5, 7.2, 9, and 11-12 MHz in the airborne transfer function (Figure 42) appear to represent half wavelength dimensions on the CV-580 aircraft (6:6). The transfer functions from the current pulse simulation (Figures 29, 30, and 31) all have lobes at 6, 8, 16, and 20 MHz, which seem to correspond to direct and multiple dimensions of the test cylinder with the coaxial return path. Assuming a propagation velocity through the test cylinder that is 80 percent the speed of light, the spikes at 8 MHz represents a half wavelength dimension of 15 meters, which is approximately the length of the coaxial return path. A multiple of this particular spike occurs at

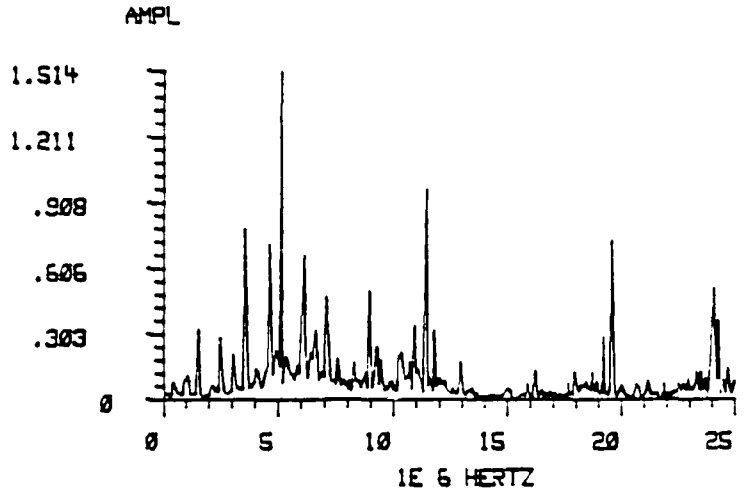


Figure 42. Transfer Function of External H-Field Response for CV-580 Airborne Lightning Measurement.

16 MHz and reflects a full wavelength dimension of the coaxial return path. The test cylinder itself is represented similarly by the lobes occuring at 6 and 20 MHz, which correspond approximately to 40 and 12 meters, respectively. The two prominent spikes for the shock-excitation case, shown in Figure 32, represent approximately 4 meters for the spike at 57 MHz and 3.6 meters for the spike at 67 MHz.

5. Conclusions and Recommendations

Based on the experimental results obtained during this thesis and presented in Chapter 4, several conclusions can be drawn which answers the questions initially posed for this research effort. One of the goals of this thesis was to compare the transients produced by the current pulse and shock-excitation simulation methods with swept frequency continuous wave measurements. The comparisons were made with respect to external H-field transients that were linearly scaled to the full threat-level current waveform. The results, shown in Figure 38, indicate that the SFCW linear scaled measurement has the largest predicted H-field transient of all of the test techniques investigated in this thesis. The results from both oscillatory current pulse methods have the lowest predicted H-field responses. From these results, one can see the problems of linearly scaling low-level transients. The SFCW method, which uses very low energy levels of approximately 25 watts, appear to overestimate the full threat-level response. The problem seems to be the extreme extrapolation that is necessary to scale the SFCW measurement to energy levels that are associated with a threat current waveform with a peak amplitude of 200 kA. This problem can also be attributed to the very large predicted H-field transient for the shock-excitation method. The measured peak current of the

shock-excitation method is approximately 1.4 kA, which is then linearly scaled to 200 kA. On the other hand, the external H-field measurement from the 100 kA oscillatory current pulse method requires a relatively small extrapolation to the full threat-level current waveform; and therefore, it appears to predict more reasonable results. This can be seen from the actual measured transients for the 100 kA oscillatory current pulse case in Table 2. From Table 2, one sees that the actual measured results for the 100 kA oscillatory current pulse are very close to the predicted full threat-level values due to the smaller extrapolation that is required. These results point out the validity of the assumption of a linear system because it tends to predict conservatively higher transient values. However, it also points out that extreme care must be exercised when analyzing these linearly extrapolated values, since scaling the measured responses overestimates the predicted values. The less the extrapolation that is necessary, the more accurate the predicted induced transient values will be (5).

In analyzing the experimental time rate-of-change results of the current pulse lightning simulation tests, one sees that the dH/dt responses produced by the current pulse tests are sufficient in replicating the airborne measurement of 3.1×10^9 A/m/s. However, the current pulse method was not able to achieve the dE/dt responses of the airborne

case, which is 3.7 x 10^{12} V/m/s. The difference is small; the dE/dt transients are below the airborne event by approximately a factor of 3. It appears that only the shock-excitation technique was able to generate the peak dE/dt responses that is sufficiently high enough to exceed the CV-580 airborne lightning strike measurement.

In terms of electric field transients, the in-flight measurements of the CV-580 recorded maximum E-field transients of about 200 kV/m (18:154). From results of the peak external E-field responses shown in Table 2, only the shock-excitation technique is able to simulate airborne E-field transient. The shock-excitation test method produces a peak E-field transient of 241 kV/m for the solid aluminum panel configuration which exceeds the measured airborne response.

Therefore, in order to generate the electric field and the time rate-of-change of the electric field that are measured for the aircraft/lightning interaction event, it appears to be necessary to employ the shock-excitation test method. However, these values for the electric field and the time rate-of-change of the electric field can also be achieved through the current pulse simulation technique by linearly extrapolating the measured responses. The full threat-level responses, as shown in Table 1, are obtained in this thesis by deriving the transfer function of the field response with respect to the injected excitation current,

and then folding the full threat-level current waveform into the transfer function. It is important that one takes into account the degree of overestimation that occurs when linearly scaling the responses to the full threat-level. The amount by which the induced transients are to be extrapolated in the analysis should be minimized. One option, which may be impractical to use on large aircraft, is to incorporate very high current generators in the current pulse simulation tests.

The effects that the current pulse test method is not able to simulate are the effects of nearby lightning and the effects of the approaching stepped leader of a lightning strike. However, the shock-excitation technique simulates these effects, respectively, by the rapidly changing E-field at the input spark gap and by the charging phase of the simulation. The electric field responses generated by the shock-excitation technique are very similar to those measured by the CV-580 in-flight tests. A typical analog measurement of the E-field during a lightning strike to an aircraft, which is shown in Figure 43, resembles very closely to the results of the charging and discharging phases of the shock-excitation tests.

In terms of current, magnetic field, and electric field transients, the experimental results of this thesis indicate that the current pulse technique is able to reproduce the effects measured during in-flight lightning strikes to the

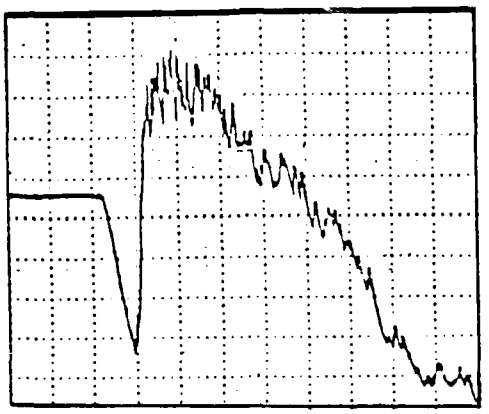


Figure 43. Typical E-Field Waveform During a Lightning Strike to Airborne CV-580 Aircraft.

CV-580 aircraft. An important note is that the comparisons conducted in this thesis were of a limited number of parameters which only included their peak magnitudes and their peak time rate-of-changes.

The experimental results of this thesis, however, are not able to answer the question of whether the the current pulse technique alone is sufficient to assess the susceptiblity and vulnerability of an aircraft to the lightning threat. The question in this case is whether the prereturn stroke phase of the lightning strike presents a unique hazard to aircraft (4:6). If it does, then the next question is whether the prereturn stroke phase can be neglected if the aircraft is tested and protected using the results from current pulse testing. These questions on lightning simulation testing require further investigation.

Should the current pulse method prove to be inadequate, then the shock-excitation technique can be incorporated to complement lightning simulation testing.

Recommendations

This thesis effort took a first step in assessing the capabilities of lightning simulation techniques by comparing the electrical parameters to airborne lightning strike measurements. There are several areas that should be investigated in future studies lightning simulation. Further comparison and analysis of the external and internal measurements of the electric and magnetic field responses should be examined for the various lightning simulation techniques. This study can include analysis of the electric and magnetic field responses for different composite aircraft structures.

A possible follow on thesis in assessing lightning simulation would be to calibrate the induced transients produced by lightning simulation in terms of the measured airborne lightning strike transients. The goal would then be determining a scaling function that would correlate the simulated lightning transients to the actual airborne event. The results from this study may improve the capability of lightning simulation technology to faithfully reproduce the effects of a lightning strike to flying aircraft.

Appendix A: Airborne Lightning Measurements

This appendix discusses the characterization program where transient responses were recorded on a specially instrumented lightning research aircraft during an actual lightning strike. During 1984 and 1985, AFWAL/FIESL, working with the FAA, U.S. Navy, NASA, and ONERA, conducted an airborne lightning characterization program. The program measured and recorded skin current distributions and electromagnetic fields resulting from direct lightning attachments to a flying aircraft. A CV-580 aircraft, provided by the FAA, was instrumented by AFWAL/FIESL and flown in and near active Florida thunderstorms at altitudes between 1,800 and 18,000 feet.

Aircraft Instrumentation

The CV-580 was instrumented with a total of 27 sensors (16:2). The instrumentation of interest for this thesis are the externally mounted current shunts, electric field sensors, and magnetic field sensors. The current shunts were mounted on the right wing tip (IRW) and the left wing tip (ILW) of the CV-580 aircraft (1:2). For the test flights during 1985, additional current shunts were mounted on top of the vertical stabilizer (IVS) and in a tail boom (ITB) behind the vertical stabilizer (1:2).

Derivative magnetic field (surface current) sensors were mounted on top of the forward fuselage (JSFF), the aft fuselage (JSAF), and the left wing between the fuselage and

the engine pod (JSTLW). Surface current sensors were also located between the fuselage and the engine pods on the bottom of the left (JSLW) and right (JSRW) wings. Derivative electric field (displacement current) sensors were mounted on top of the forward fuselage (JNFF) and on top of the right wing (JNTRW), between the fuselage and the engine pod. Derivative electric field sensors were also placed on the bottom of the right (JNRW) and left (JNLW) wing tips (1:2). Figure 44 shows the placement of the various sensors on the CV-580 aircraft.

The high frequency data from the sensors were recorded by six Textronix 7612D waveform digitizers, each with two input channels. The digitizers were set to record 2048 samples at 5 nanosecond intervals. This provided a recording window of 10.24 microseconds of digital data with an upper bandwidth of 100 MHz. The low frequency data, DC to 500 kHz in the FM channels and 400 Hz to 2 MHz in the direct channels, were recorded continuously by a 28-channel Honeywell 101 analog recorder.

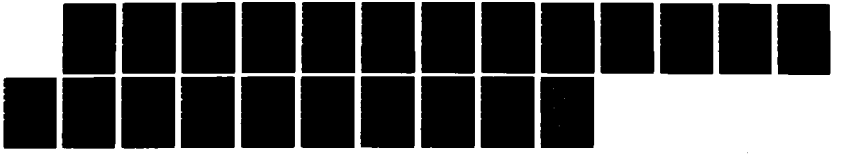
Ground Station

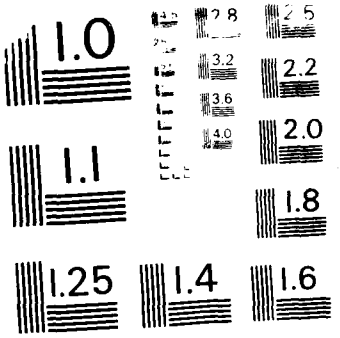
Ground station measurements were also conducted during the lightning characterization program. A ground station trailer, which was located north of Kennedy Space Center, was instrumented with two flush plate electric field antennas and two crossed-loop magnetic field sensors (16:2).

AD-A190 576 EXPERIMENTAL COMPARISON OF LIGHTNING SIMULATION TECHNIQUES TO CV-580 AIRB (U) AIR FORCE INST OF TECH WRIGHT-PATTERSON AFB OH SCHOOL OF ENGI R M BRAZA

2/2

UNCLASSIFIED DEC 87 AFIT/GE/ENG/87D-5 F/G 4/1 NL





MICROCOPY RESOLUTION TEST CHART
NATIONAL BUREAU OF STANDARDS-1963-A

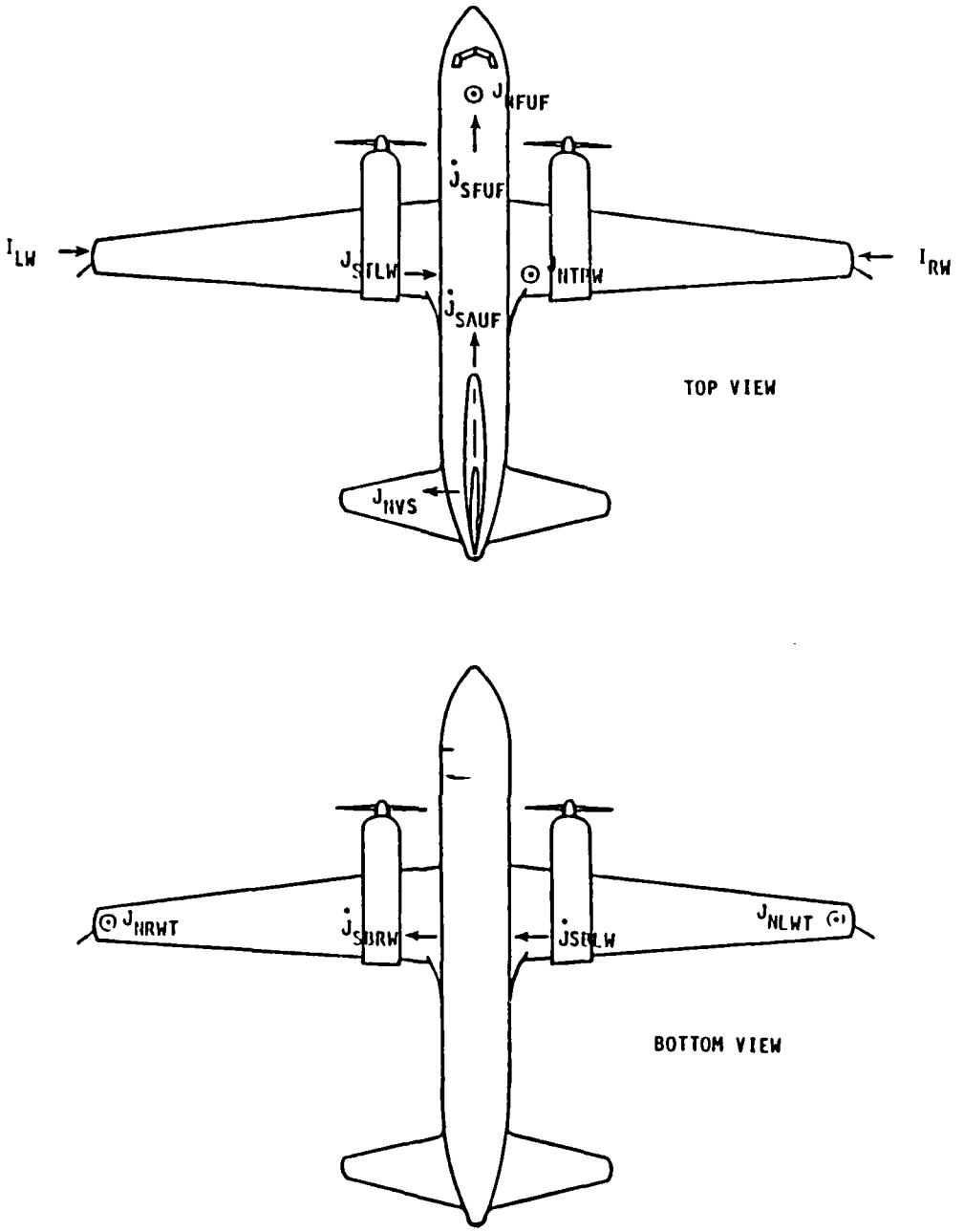


Figure 44. Sensor Locations on CV-580 Aircraft.

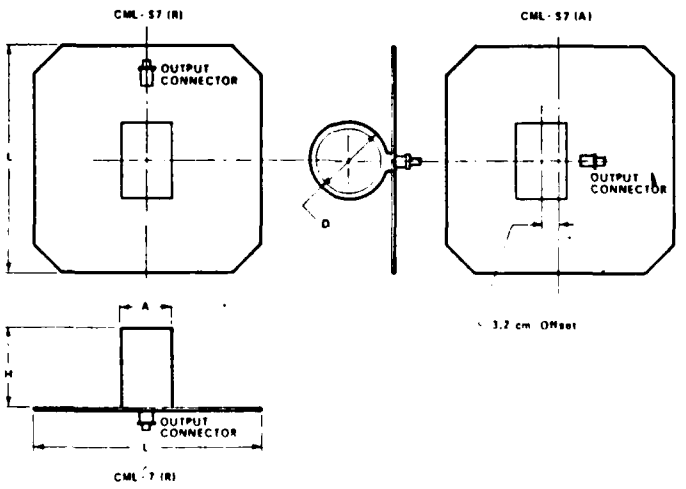
Appendix B: Sensor Specifications

As presented in Chapter 3, various magnetic and electric field sensors were used during the lightning simulation measurements of this thesis. This appendix contains the data sheets of the specifications for the EG&G sensors used. The sensor data sheets include the Cylindrical Moebius Loop (CML), Multi-Gap Loop (MGL), Hollow Spherical Dipole (HSD), Flush Plate Dipole (FPD), and Asymptotic Conical Dipole (ACD) sensors.

SPECIFICATIONS

Parameter	CML-7 or CML-S7
A_{eq} (m^2)	2×10^{-2}
Frequency Response (3 dB point)	38 MHz
Risetime (10-90%)	9 ns
Maximum Output	4 kV (with TCC)
Maximum Field Change	2×10^5 tesla/sec
Output Connector	TCC*
Mass	1.0 kg
Dimensions (cm)	
L	35.6
D	11.9
H	12.4
A	6.4

*100-ohm twinaxial connector (Data Sheet 1340); Two 50-ohm SMA connectors optional.



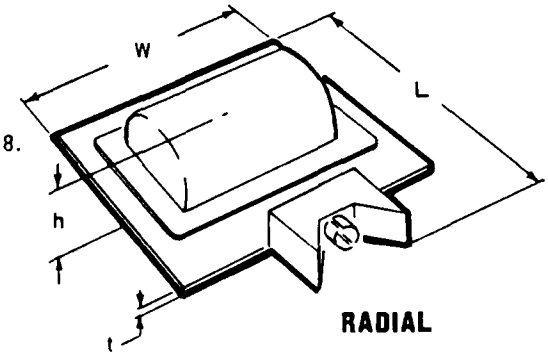
(Data and Specifications Subject to Change without Notice)

SPECIFICATIONS

Parameter	MGL-S4	MGL-S5	MGL-S7	MGL-S8
A_{eq} (m^2)	1×10^{-2}	1×10^{-3}	1×10^{-4}	1×10^{-5}
Frequency Response (3 dB pt)	> 230 MHz	> 700 MHz	> 1.8 GHz	> 5 GHz
Risetime ($T_{r\ 10-90}$)	≤ 1.5 ns	≤ 0.5 ns	≤ 0.2 ns	≤ .07 ns
Maximum Output	5 kV	5 kV	1.0 kV	150V
Maximum Field Change (Teslas/sec)	5×10^5	5×10^6	1×10^7	1.5×10^7
Output Connector	GR874L-50Ω	GR874L-50Ω	ARM2054-0000	ARMM 4064-0000
Mass	4.5 kg	2.7 kg	80 g	15 g
Dimensions (cm)				
L	41.4	31.5	10.4	7.62
W	36.3	25.4	5.6	2.54
h	13.2	6.1	2.3	1.38
t	0.32	0.38	0.25	0.1

Note: Ground plane dimensions are somewhat different between Radial and Axial versions. The larger (radial) dimensions are listed. Axial or Radial output specified by designations MGL-SN(A) and MGL-SN(R), respectively, where N = 4, 5, 7, or 8.

Note: "h" for Models S7 and S8 is connector height.



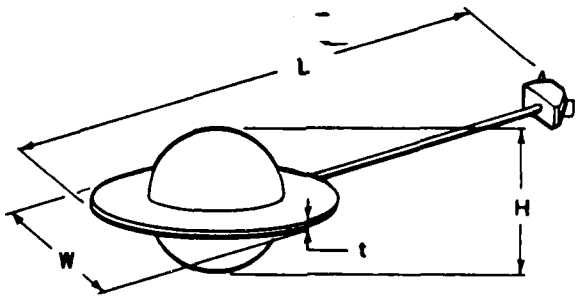
RADIAL

(Data and Specifications Subject to Change without Notice)

SPECIFICATIONS

Parameter	HSD-2 (R)	HSD-4 (R)
A_{eq} (m^2)	1×10^{-1}	1×10^{-2}
Frequency Response (3 dB Point)	> 45 MHz	> 150 MHz
Risetime ($T_{r\ 10\text{-}90}$)	≤ 7.4 ns	≤ 2.3 ns
Maximum Output	5 kV	5 kV
Output Connector	TCC - 100 ohm*	TCC - 100 ohm*
Mass	2.15 kg	0.59 kg
Dimensions (cm)		
L	62.5	44.7
W	28.5	8.9**
H	20.6	6.9
t	0.3	0.16

*100-ohm Twinaxial Connector (EG&G Data Sheet 1340)
**Connector width is greater than W on Model 4 (11.7 cm)



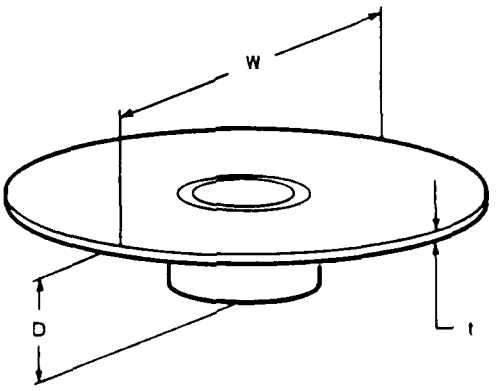
NOTES:

(1) During use, this sensor must be supported by dielectric materials and positioned at least two sensor diameters from any conducting surfaces.
(2) A DLT-96 balun (EG&G Data Sheet 1300) can be used to transform 100-ohm balanced output to 50-ohm unbalanced output for telemetry and recording.

(Data and Specifications Subject to Change without Notice)

SPECIFICATIONS:

	FPD-1	FPD-2
A_{eq} (m^2)	1×10^{-2}	2×10^{-2}
Frequency Response (3 dB point)	> 350 MHz	>70 MHz
Risetime ($T_{r\ 10\text{-}90}$)	< 1 ns	<5 ns
Maximum Output	5 kV	5 kV
Output Connector	GR874L (50 ohms)	GR874L (50 ohms)
Mass	4 kg	2 kg
Dimensions (cm)		
W	43.2	28.3
t	1.0	0.5
D	5.4	5.2



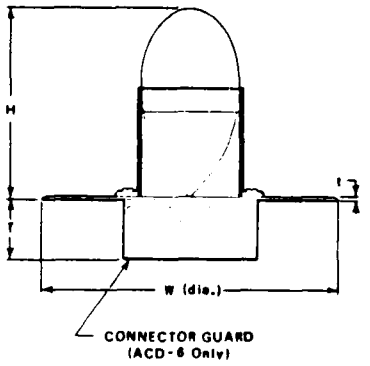
(Data and Specifications Subject to Change without Notice)

SPECIFICATIONS

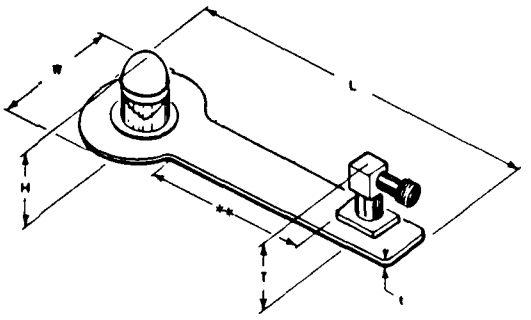
	ACD-S1(R)*	ACD-1(A)*	ACD-3(A)	ACD-S3(R)	ACD-5(R)	ACD-6(A)	ACD-9(A)
$A_{eq}(m^2)$	1×10^{-4}	1×10^{-4}	1×10^{-2}	1×10^{-2}	1×10^{0}	1×10^{-1}	1×10^{-3}
Frequency Response (3-dB point)	>11.0 GHz	>11.0 GHz	>1.10 GHz	>1.10 GHz	>110 MHz	>350 MHz	>3.5 GHz
Risetime (T_r 10-90)	<0.032 ns	<0.032 ns	<0.32 ns	<0.32 ns	<3.2 ns	<1.0 ns	<0.10 ns
Maximum Output	125 V	125 V	1000 V	5 kV	5 kV	5 kV	1000 V
Output Connector	OSSM 274 50Ω coaxial	ARMM 4052-0000	ARM 2052-0000	GR** 874L 50Ω	GR 874L 50Ω	GR 874L 50Ω	ARM 2052-0000
Mass	12 g	15 g	327 g	550 g	60 kg	1.3 kg	60 g
Dimensions (cm)							
L	7.62	---	---	22.2	152.40	---	---
W	2.54	2.54	13.97	14.3	121.92	28.2	5.59
H	0.59	0.59	5.16	5.16	49.14	15.56	1.79
t	0.10	0.10	0.254	0.24	0.64	0.32	0.236
T	1.32	1.18	1.82	3.19	4.13	6.03	1.82

* Axial or Radial Output Specified by Designations ACD-N(A) or ACD-N(R), Respectively, where N = 1 or 3.
**OSM Connector Available on Request.

AXIAL



RADIAL



** Flexible Ground Plane Version has a Thin Plate and Coaxial Wire in this Section.

(Data and Specifications Subject to Change without Notice)

Appendix C: Data Acquisition Computer Program

This appendix contains a complete listing of the computer program, written by AFWAL/FIESL, that was used for data acquisition during the current pulse and shock-excitation lightning simulation tests on the Lightning Test Cylinder. The program controls the two 2-channel Tektronix 7612D waveform digitizers and performs data reduction. The data is stored on 9-track magnetic tape. The program runs on the Digital PDP 11/34 using the TEK SPS BASIC Signal Processing Package.

```
1 REM   DATA ACQUISITION PROGRAM FOR
2 REM   CURRENT PULSE LIGHTNING SIMULATION
3 REM   AND SHOCK-EXCITATION LIGHTNING SIMULATION
10 PRINT 'WAVEFORMS FROM TAPE (Y OR N)':\INPUT Y$
11 IF Y$='Y' THEN GOTO 4400
12 LOAD 'GPI','MT'
13 SIFLIN @0,'IFC'
14 SIFCOM @0,'DCL'
15 SIFTO @0,500
20 PRINT 'INITIALIZE SYSTEM (Y OR N) ':\INPUT Y$
21 IF Y$='Y' THEN GOTO 1000
22 GOTO 1050
100 REM START OF PROGRAM**********
101 GOSUB 4000\REM SET UP FILE NAME AND NUMBER
110 PRINT 'SET UP DIGITIZERS (Y OR N)':\INPUT Y$
111 IF Y$='Y' THEN GOSUB 2000
115 TT$=FT$\PRINT 'TEST NAME ':FT$;\INPUT FT$\IF FT$='S' THEN FT$=TT
$
116 PRINT FT$\IF FT$='R' THEN GOTO 1050
117 PRINT 'ARM SYSTEM (Y OR N)':\INPUT Y$
118 IF Y$='N' THEN GOTO 125
120 FOR I=33 TO 34
121 PUT 'ARM A,B' INTO @0,I,96
122 PUT 'POS 0.0' INTO @0,I,96+1
123 PUT 'POS 0.0' INTO @0,I,96+2
124 NEXT I
125 PRINT 'DIGITIZERS ARMED (Y TO READ)(N TO REARM)':\INPUT Y$
126 IF Y$='N' THEN GOTO 120
127 GOSUB 2100
130 PRINT 'GRAPH DATA (Y OR N)':\INPUT Y$
131 IF Y$='Y' THEN GOSUB 3000
135 PRINT 'SAVE DATA (Y OR N)';\INPUT Y$
136 IF Y$='Y' THEN GOSUB 4100
137 PRINT 'INDIVIDUAL PLOTS (Y OR N)';\INPUT Y$
138 IF Y$='Y' THEN GOSUB 3200
139 GOTO 115
1000 REM INITIALIZE SYSTEM **********************************
1001 SI$='5E-9'
1002 SI=VAL(SI$)
1005 LA=32\TA=64\SA=96
1006 PL$='RIN LOW; CPL AC; POS 0.0; V/D .1'
1007 PR$='RIN LOW; CPL AC; POS 0.0; V/D .1'
1008 TA$='TMBS A;MODE PRE,512;LTC RIGHT;SBPT 0,'&SI$
1009 TB$='TMBS B;MODE PRE,512;LTC RIGHT;SBPT 0,'&SI$
1010 TR$='LTC RIGHT;CPL DC;SRC EXT;LEV 25'
1020 TT$=DT$\PRINT 'DATE ':DT$;\INPUT DT$\IF DT$='S' THEN DT$=TT$
1021 TIME TT$\PRINT 'TIME ':TT$;\INPUT TM$\IF TM$='S' THEN TM$=TT$
```

```
1022 SETTIME TM$
1023 SETDATE DT$
1024 TIME T$\DATE D$
1025 PRINT 'TODAY IS ':D$:'   TIME IS ':T$
1027 AP$='N'
1030 REM SET UP WAVEFORM ARRAYS
1031 DELETE AA,BB,CC,DD,WA,WB,WC,WD
1032 H$='SEC'\VV$='VOLTS'\VA$='AMPS'
1040 WAVEFORM WA IS AA(2047),SI,H$,VA$
1041 WAVEFORM WB IS BB(2047),SI,H$,VA$
1042 WAVEFORM WC IS CC(2047),SI,H$,VA$
1043 WAVEFORM WD IS DD(2047),SI,H$,VA$
1050 REM NAME AND SCALE
1051 ZA$=NA$\PRINT '#1 NAME = ':ZA$:\INPUT NA$\IF NA$='S' THEN NA$=Z
A$
1052 PRINT '#1 SCALE =':SA:\INPUT ZA$\IF ZA$<>'S' THEN SA=VAL(ZA$)
1054 ZA$=NB$\PRINT '#2 NAME = ':ZA$:\INPUT NB$\IF NB$='S' THEN NB$=Z
A$
1055 PRINT '#2 SCALE =':SB:\INPUT ZA$\IF ZA$<>'S' THEN SB=VAL(ZA$)
1057 ZA$=NC$\PRINT '#3 NAME = ':ZA$:\INPUT NC$\IF NC$='S' THEN NC$=Z
A$
1058 PRINT '#3 SCALE =':SC:\INPUT ZA$\IF ZA$<>'S' THEN SC=VAL(ZA$)
1060 ZA$=ND$\PRINT '#4 NAME = ':ZA$:\INPUT ND$\IF ND$='S' THEN ND$=Z
A$
1061 PRINT '#4 SCALE =':SD:\INPUT ZA$\IF ZA$<>'S' THEN SD=VAL(ZA$)
1063 PRINT CHR(27):CHR(91):'2J' _
1064 PRINT CHR(27):CHR(91):'1H'
1065 PRINT '#1',NA$,SA
1066 PRINT '#2',NB$,SB
1067 PRINT '#3',NC$,SC
1068 PRINT '#4',ND$,SD
1099 GOTO 100
2000 REM SET-UP DIGITIZERS ********************************
2002 UT=LA+1
2004 PUT PL$ INTO @0,UT,96+1
2006 PUT PR$ INTO @0,UT,96+2
2008 PUT TA$ INTO @0,UT,96
2010 PUT TB$ INTO @0,UT,96
2012 PUT TR$ INTO @0,UT,96
2013 SIFCOM @0,UT,96,'GTL'
2016 UT=UT+1
2018 IF UT<LA+3 THEN GOTO 2004
2019 PRINT 'MAKE ANY CHANGES NOW'
2020 RETURN
2100 REM READ DATA AND SCALE **********************************
2101 TIME T$\DATE D$
2102 UT=1\GOSUB 2150
2103 AA=A-128
```

```
2104 VA=VAL(SEG(VA$,4,LEN(VA$)))
2105 BB=B-128
2106 VB=VAL(SEG(VB$,4,LEN(VB$)))
2107 UT=2\GOSUB 2150
2108 CC=A-128
2109 VC=VAL(SEG(VA$,4,LEN(VA$)))
2110 DD=B-128
2111 VD=VAL(SEG(VB$,4,LEN(VB$)))
2118 RETURN
2150 REM READ DIGITIZER (UT=UNIT #)
2155 PRINT UT\DELETE A,B
2160 PUT 'READ A' INTO @0,32+UT,96
2165 READBI A FROM @0,64+UT,96
2166 PUT 'V/D?' INTO @0,32+UT,96+1
2167 GET VA$ FROM @0,64+UT,96+1
2170 PUT 'READ B' INTO @0,32+UT,96
2175 READBI B FROM @0,64+UT,96
2176 PUT 'V/D?' INTO @0,32+UT,96+2
2177 GET VB$ FROM @0,64+UT,96+2
2180 RETURN
3000 REM GRAPH DATA ****************************************
3001 PRINT CHR(27);CHR(91);'2J'
3002 PRINT CHR(27);CHR(91);'1;1H'
3003 PRINT CHR(27);'1'
3004 PAGE
3005 DELETE GG,WG
3006 WAVEFORM WG IS GG(2047),SI,H$,GV$
3007 UT=1
3008 GV$=''
3010 GOTO UT OF 3020,3025,3030,3035,3040
3020 VIEWPORT 100,450,500,700
3021 SG=(SA*VA)/32
3022 GG=AA*SG
3023 GV$=NA$
3024 GOTO 3100
3025 VIEWPORT 550,900,500,700
3026 SG=(SB*VB)/32
3027 GG=BB*SG
3028 GV$=NB$
3029 GOTO 3100
3030 VIEWPORT 100,450,150,350
3031 SG=(SC*VC)/32
3032 GG=CC*SG
3033 GV$=NC$
3034 GOTO 3100
3035 VIEWPORT 550,900,150,350
3036 SG=(SD*VD)/32
3037 GG=DD*SG
```

```
3038 GV$=ND$
3039 GOTO 3100
3040 RESETG
3041 MOVE 10,40\PRINT 'TEST NAME'
3042 MOVE 400,40\PRINT 'FILE NAME','   DATE','  TIME'
3043 MOVE 10,10\PRINT FT$
3044 MOVE 400,10\PRINT FF$,D$,T$
3045 IF AP$='N' THEN GOTO 3050
3046 PRINT CHR(27):CHR(23)
3047 GOTO 3051
3050 WAIT
3051 PAGE
3052 PRINT CHR(27):'2'
3053 RETURN
3100 REM GRAPH DATA ***********************************
3102 PRINT CHR(27):'1'
3105 WINDOW 0,SI*2000,SG*(-128),SG*128
3106 SETGR VIEW,WIND,TICS 5,4,GRAT 4,4,2,2
3110 GRAPH WG
3111 UT=UT+1
3112 GOTO 3010
3200 REM GRAPH INDIVIDUAL PLOTS
3201 PRINT 'SELECT PLOT (1-2-3-4)(0 TO RETURN)':\INPUT GN\IF GN=0 TH
EN RETURN
3202 PRINT CHR(27):CHR(91):'2J'
3203 PRINT CHR(27):CHR(91):'1H' —
3204 PRINT CHR(27):'1'
3205 PAGE
3206 DELETE GG,WG
3207 WAVEFORM WG IS GG(2047),SI,H$,GV$
3210 GOTO GN OF 3215,3220,3225,3230
3215 SG=(SA*VA)/32
3216 GG=AA*SG
3217 GV$=NA$
3218 GOTO 3234
3220 SG=(SB*VB)/32
3221 GG=BB*SG
3222 GV$=NB$
3223 GOTO 3234
3225 SG=(SC*VC)/32
3226 GG=CC*SG
3227 GV$=NC$
3228 GOTO 3234
3230 SG=(SD*VD)/32
3231 GG=DD*SG
3232 GV$=ND$
3234 GG=GG-MEA(GG(0:50))
3235 VIEWPORT 100,900,150,700
```

```
3236 WINDOW 0,SI*2000,SG*(-128),SG*128
3237 SETGR VIEW,WIND,TICS 5,4,GRAT 4,4,2,2
3238 GRAPH WG
3240 RESETG
3241 MOVE 10,40\PRINT 'TEST NAME'
3242 MOVE 400,40\PRINT 'FILE NAME','   DATE','  TIME'
3243 MOVE 10,10\PRINT FT$
3244 MOVE 400,10\PRINT FF$,D$,T$
3245 WAIT
3246 PAGE
3247 PRINT CHR(27);'2'
3250 PRINT 'INT OR FFT OR N';\INPUT Y$
3251 IF Y$='INT' THEN GOSUB 3300
3252 IF Y$='FFT' THEN GOSUB 3400
3253 GOTO 3200
3300 DELETE RL,RR
3301 WAVEFORM RR IS RL(2047),SI,HR$,VR$
3302 INT WG,RR
3303 HR$=H$
3304 VR$=GV$&' INTEGRATED'
3305 GOTO 3430
3400 REM FFT OF DISPLAYED WAVEFORM
3405 DELETE RL,IM,RR,II
3410 WAVEFORM RR IS RL(1024),FI,HR$,VR$
3415 WAVEFORM II IS IM(1024),FI,HI$,VI$
3420 RFFT WG,RR,II
3425 POLAR RR,II
3426 RL(0)=MIN(RL)
3427 HR$='FREQ IN MEG HZ'
3430 PRINT CHR(27);CHR(91);'2J'
3435 PRINT CHR(27);CHR(91);'1H'
3440 PRINT CHR(27);'1'
3445 PAGE
3450 VIEWPORT 100,900,150,700
3460 SETGR VIEW,GRAT 4,4,2,2
3470 GRAPH RR
3475 RESETG
3480 MOVE 10,40\PRINT 'TEST NAME'
3485 MOVE 400,40\PRINT 'FILE NAME','  DATE','  TIME'
3490 MOVE 10,10\PRINT FT$
3495 MOVE 400,10\PRINT FF$,D$,T$
3499 WAIT 1000
3500 WAIT
3505 PAGE
3510 PRINT CHR(27);'2'
3515 RETURN
4000 REM SET UP FILE NAME FOR SAVE
4002 REM FN$=FILE NAME
```

```
4004 REM FN=FILE NUMBER
4006 REM FF$=COMPLETE NAME FOR FILE TO BE SAVED
4007 TT$=FN$\PRINT 'FILE = ';FF$\INPUT FN$
4008 IF FN$='S' THEN GOTO 4040
4009 IF LEN(FN$)<7 THEN GOTO 4011
4010 PRINT 'FILE NAME TOO LONG'\GOTO 4007
4011 SS$='?'
4012 FOR I=1 TO LEN(FN$)
4014 TC=ASC(SEG(FN$,I,I))
4016 IF TC>47 THEN IF TC<58 THEN GOTO 4022
4018 IF TC>64 THEN IF TC<91 THEN GOTO 4022
4020 GOTO 4024
4022 SS$=SS$&CHR(TC)
4024 NEXT I
4026 FN$=SEG(SS$,2,LEN(SS$))
4028 PRINT 'FILE NUMBER';\INPUT FN
4029 IF FN<1000 THEN GOTO 4031
4030 PRINT 'FILE NUMBER TOO BIG'\GOTO 4028
4031 SS$='00'&STR(FN)
4032 FF$=FN$&'.'&SEG(SS$,LEN(SS$)-2,LEN(SS$))
4034 PRINT 'FILE NAME =';FF$
4035 RETURN
4040 FN$=TT$
4041 GOTO 4034
4100 REM SAVE DATA
4109 PRINT 'FILE NAME =';FF$
4110 OPEN #1 AS MT:/F,FF$ FOR WRITE WITH 4
4111 WRITE #1,FF$,FN$,FN,FT$,D$,T$
4112 WRITE #1,NA$,WA,SA,VA
4113 WRITE #1,NB$,WB,SB,VB
4114 WRITE #1,NC$,WC,SC,VC
4115 WRITE #1,ND$,WD,SD,VD
4116 FN=FN+1
4117 SS$='00'&STR(FN)
4118 FF$=FN$&'.'&SEG(SS$,LEN(SS$)-2,LEN(SS$))
4119 CLOSE #1
4120 PRINT 'NEXT FILE IS ';FF$
4121 RETURN
4400 REM READ WAVEFORMS FROM MAG TAPE
4405 DELETE AA,BB,CC,DD,WA,WB,WC,WD
4410 WAVEFORM WA IS AA(2047),SI,H$,VA$
4415 WAVEFORM WB IS BB(2047),SI,H$,VA$
4420 WAVEFORM WC IS CC(2047),SI,H$,VA$
4425 WAVEFORM WD IS DD(2047),SI,H$,VA$
4430 PRINT 'AUTO PLOT (Y OR N)';\INPUT AP$
4431 RELEASE 'MT'
4435 LOAD 'MT'
4440 REWIND MT:
```

```
4445 GOSUB 4000
4450 OPEN #1 AS MT:/F,FF$ FOR READ
4455 READ #1,FF$,FN$,FN,FT$,D$,T$
4460 READ #1,NA$,WA,SA,VA
4465 READ #1,NB$,WB,SB,VB
4470 READ #1,NC$,WC,SC,VC
4475 READ #1,ND$,WD,SD,VD
4480 CLOSE #1
4481 GOSUB 3000
4482 IF AP$='Y' THEN GOTO 4490
4485 PRINT 'INDIVIDUAL PLOTS (Y OR N)':\INPUT Y$\IF Y$='Y' THEN GOSU
B 3200
4490 FN=FN+1\SS$='00'&STR(FN)
4495 FF$=FN$&'.'&SEG(SS$,LEN(SS$)-2,LEN(SS$))
4496 IF AP$='Y' THEN GOTO 4450
4500 PRINT 'NEXT FILE (Y OR N) ':FF$\INPUT Y$
4505 IF Y$='Y' THEN GOTO 4450
4510 GOTO 4445
```

BIBLIOGRAPHY

1. Burket, H.D. "Comparison of Electromagnetic Measurements on an Aircraft from Direct Lightning Attachment and Simulated Nuclear Electromagnetic Pulse," 1986 International Aerospace and Ground Conference on Lightning and Static Electricity. Paper No. 17: 1-5. Dayton OH, June 1986.

2. Butters, W.G. *et al.* Assessment of Lightning Simulation Test Techniques: Final Report - Part 1, July 1980 - October 1981. McDonnell Aircraft Company, October 1981 (AFWAL-TR-81-3075).

3. Clifford, D.W., K.E. Crouch, and E.H. Schulte. "Lightning Simulation and Testing," IEEE Transactions on Electromagnetic Compatibility, Vol. EMC-24, No. 2: 09-224 (May 1982).

4. Clifford, D.W. and K.S. Zeisel. "Evaluation of Lightning-Induced Transients in Aircraft Using High-Voltage Shock Excitation Techniques," Proceedings of the 1979 IEEE International Symposium on Electromagnetic Compatibility. San Diego CA, 9-11 October 1979.

5. Hebert, Captain J.L. Lightning Analysis and Characterization Engineer. Personal Correspondence. AFWAL/FIESL, Wright-Patterson AFB OH, October 1987.

6. Hebert, J.L., J.S. Reazer, and J.G. Schneider. "Current Levels and Distributions on an Aircraft During Ground Lightning Simulation Tests and In-Flight Lightning Attachments," 1986 International Aerospace and Ground Conference on Lightning and Static Electricity. Paper No. 19: 1-21. Dayton OH, June 1986.

7. Hebert, J.L., M.P. Hebert, L.C. Walko, *et al.* "Pulsed Power Applications in Lightning Protection Qualification Testing," Proceedings of the 6th International Pulsed Power Conference. Arlington VA, June 1987.

8. Hebert, J.L. and P.L. Rustan. "Lightning Strikes to Aircraft at Low Altitudes," Proceedings of the 2nd International Meteorological Conference on Aviation Weather. Montreal Canada, June 1986.

9. Mabee, D.S. Validation of GEMACS for Modeling of Lightning Induced Electromagnetic Fields. Master's Thesis. Air Force Institute of Technology, Wright-Patterson AFB OH, December 1987.

10. McCormick, W., K.J. Maxwell, and R. Finch. Analytical and Experimental Validation of the Lightning Transient Analysis Technique: Final Report, March - November 1977. Technology Incorporated, Dayton OH, March 1978 (AD-A063991).

11. Melander, B.G. "Effects of Tower Characteristics on Lightning Arc Current Measurements," 1984 International Aerospace and Ground Conference on Lightning and Static Electricity. Paper No. 34: 1-12. Orlando FL, June 1984.

12. Perala, R.A. and G.A. DuBro. Assessment Methodology of the Lightning Threat to Advanced Aircraft. Electromagnetic Applications, Inc., Denver CO and Air Force Wright Aeronautical Laboratories, Wright-Patterson AFB OH.

13. Perala, R.A. *et al.* "Electromagnetic Interactions of Lightning with Aircraft," IEEE Transactions on Electromagnetic Compatibility, Volume EMC-24, No. 2: 173-203 (May 1982).

14. Plumer, J.A. and J.D. Robb. "The Direct Effects of Lightning on Aircraft," IEEE Transactions on Electromagnetic Compatibility, Volume ENC-24, No. 2: 158-172 (May 1982).

15. Robb, J.D. Atmospheric Electricity Hazards Analytical Model Development and Applications, Volume II: Simulation of the Lightning/Aircraft Interaction Event: Final Report, August 1979 - June 1981. Contract F-33615-79-C-3412. Electro-Magnetic Applications, Inc., Denver CO, June 1981 (AD-A114016).

16. Reazer, J.S. and R.D. Richmond. "Simultaneous Airborne and Ground Measurement of Low Altitude Cloud-to-Ground Lightning Strike on CV-580 Aircraft," 1986 International Aerospace Conference on Lightning and Static Electricity. Paper No. 16: 1-3. Dayton OH, June 1986.

17. Rustan, P.L. "A Review of Aerospace and Ground Lightning Threat Characteristics and Applications," 1986 International Aerospace and Ground Conference on Lightning and Static Electricity: Sec 1, 1-8 (24-26 June 1986).

18. Rustan, P.L., B.P. Kuhlman, H.D. Burket, J. Reazer, and A. Serrano. Low Altitude Lightning Attachment to an Aircraft. Interim Report, October 1983 - February 1985. Wright-Patterson AFB, OH: Flight Dynamics Laboratory, Air Force Wright Aeronautical Laboratories (AFWAL/FIESEL), May 1987.

19. Uman, M.A. Lightning. New York: Dover Publications, Inc., Dover Edition, 1984.

20. Uman, M.A. and E.P. Krider. "A Review of Natural Lightning: Experimental Data and Modeling," IEEE Transactions on Electromagnetic Compatibility, Volume EMC-24, No. 2: 79-112 (May 1982).

21. Walko, L.C. and J.G. Schneider. "Full Scale Lightning Test Technique," FAA/NASA Symposium on Lightning Technology, NASA Conference Publication 2128. 449-458. Hampton VA, April 1980.

VITA

Lieutenant Rudy M. Braza was born on 21 January 1964 in Yokosuka, Japan. He graduated from Menchville High School in Newport News, Virginia, in 1982. He attended Virginia Polytechnic Institute and State University and received the degree of Bachelor of Science in Electrical Engineering *magna cum laude* in June 1986. A member of the Virginia Tech Corps of Cadets, he received a commission in the Air Force through the ROTC program upon graduation. He entered directly into the School of Engineering, Air Force Institute of Technology, in June 1986.

—

Permanent address: 415 Eastwood Drive
Newport News, Virginia 23602

UNCLASSIFIED
SECURITY CLASSIFICATION OF THIS PAGE

REPORT DOCUMENTATION PAGE

Form Approved
OMB No 0704-0188

1a. REPORT SECURITY CLASSIFICATION UNCLASSIFIED	1b. RESTRICTIVE MARKINGS
2a. SECURITY CLASSIFICATION AUTHORITY	3. DISTRIBUTION/AVAILABILITY OF REPORT Approved for public release; Distribution Unlimited
2b. DECLASSIFICATION/DOWNGRADING SCHEDULE	
4. PERFORMING ORGANIZATION REPORT NUMBER(S) AFIT/GE/ENG/87D-5	5. MONITORING ORGANIZATION REPORT NUMBER(S)
6a. NAME OF PERFORMING ORGANIZATION School of Engineering 6b. OFFICE SYMBOL (If applicable) AFIT/ENG	7a. NAME OF MONITORING ORGANIZATION
6c. ADDRESS (City, State, and ZIP Code) Air Force Institute of Technology (AU) Wright-Patterson AFB, Ohio 45433-6583	7b. ADDRESS (City, State, and ZIP Code)
8a. NAME OF FUNDING/SPONSORING ORGANIZATION Flight Dynamics Laboratory 8b. OFFICE SYMBOL (If applicable) AFWAL/FIESL	9. PROCUREMENT INSTRUMENT IDENTIFICATION NUMBER
8c. ADDRESS (City, State, and ZIP Code) Air Force Wright Aeronautical Laboratories (AFSC) Wright-Patterson AFB, Ohio 45433-6553	10. SOURCE OF FUNDING NUMBERS PROGRAM ELEMENT NO / PROJECT NO / TASK NO / WORK UNIT ACCESSION NO

11. TITLE (Include Security Classification)
EXPERIMENTAL COMPARISON OF LIGHTNING SIMULATION TECHNIQUES TO CV-580 AIRBORNE LIGHTNING STRIKE MEASUREMENTS

12. PERSONAL AUTHOR(S)
Judy M. Braza, 2LT, USAF

13a. TYPE OF REPORT	13b. TIME COVERED	14. DATE OF REPORT (Year, Month, Day)	15. PAGE COUNT
MS Thesis	FROM _____ TO _____	1987 December	130

16. SUPPLEMENTARY NOTATION

17. COSATI CODES			18. SUBJECT TERMS (Continue on reverse if necessary and identify by block number)
FIELD	GROUP	SUB-GROUP	
01	04		Lightning; Aircraft Lightning; Simulation; Electromagnetic Coupling
01	03		

19. ABSTRACT (Continue on reverse if necessary and identify by block number)

Thesis Advisor: Randy J. Jost, Captain, USAF

20. DISTRIBUTION/AVAILABILITY OF ABSTRACT ☒ UNCLASSIFIED/UNLIMITED ☐ SAME AS RPT ☐ DTIC USERS	21. ABSTRACT SECURITY CLASSIFICATION UNCLASSIFIED
22a. NAME OF RESPONSIBLE INDIVIDUAL Randy J. Jost, Captain, USAF	22b. TELEPHONE (Include Area Code) (513) 255-3576 22c. OFFICE SYMBOL AFIT/ENG

DD Form 1473, JUN 86 — Previous editions are obsolete

SECURITY CLASSIFICATION OF THIS PAGE
UNCLASSIFIED

19. ABSTRACT

Various lightning simulation test techniques were conducted on Lightning Test Cylinder developed by the Air Force Wright Aeronautical Laboratories/Atmospheric Electricity Hazards Group (AFWAL/FIESL) and the Air Force Institute of Technology (AFIT/ENG). The experimental tests on the cylinder included swept frequency continuous wave (SFCW), current pulse, and shock-excitation. Designed to model the fuselage of an aircraft, the aluminum test cylinder is over ten meters long with a one meter diameter. To test the effects of various aircraft construction materials, the cylinder was constructed with an aperture where various composite and metal panels can be mounted. The research involved determination of the electric field and magnetic field response transfer function for each simulation test technique. With these transfer functions, analysis and comparison of the external and internal field responses were made. The results of this experimental effort on the Lightning Test Cylinder were then correlated to CV-580 airborne lightning strike measurements. Differences and similarities between the measured results are prese nted.

END

DATE

FILMED

DTIC

4/88